The Thesis Committee for Lin Yang

Certifies that this is the approved version of the following thesis:

Comparative Analysis of Lost Circulation Material Particle Size and Degradation in Drilling Fluids

APPROVED BY

SUPERVISING COMMITTEE:

Supervisor: Eric van Oort

Co-Supervisor: Arthur Hale

Comparative Analysis of Lost Circulation Material Particle Size and Degradation in Drilling Fluids

by

Lin Yang, B.S.

Thesis

Presented to the Faculty of the Graduate School of

The University of Texas at Austin

in Partial Fulfillment

of the Requirements

for the Degree of

Master of Science in Engineering

The University of Texas at Austin

May 2015

Dedication

To Liangrong Yang and Shichai Lin, my parents and my foundation.

Acknowledgements

I wish to express my sincere thanks to my supervisor, Dr. Eric van Oort, for his patient guidance and mentorship, for all the precious and valuable opportunities I have been exposed to under his supervision. I also would like to express my gratitude to Dr. Arthur Hale. I am indebted to him for sharing his expertise, wisdom, and valuable guidance.

I would like to thank Besmir Hoxha, Dr. Sriramya Duddukuri Nair, Dr. Ali Karimi and Oguz Incedalip. Without their support, encouragement, and dedicated assistance, this thesis would not have been possible. I would like to thank Iona Williams, Michelle Shuck, Xiangyu Liu, Tesse Smitherman, Glen Baum, Gary Miscoe, Daryl Nygaard, the members of Zonal Isolation Group and Drilling Rig Automation Group for their support and help throughout my graduate study. It has been a pleasure to work with these brilliant people.

I would like to express my gratitude to Dave Marshall, Ron Bland and Dennis Clapper from Baker Hughes Inc. for sharing their knowledge and offering valuable feedback for this work. I would like to thank Anjan Pandey and Rodrigo Azevedo from Mettler-Toledo International Inc., Todd Canty and Justin Halbach from JM Canty Inc. for sharing their technical expertise and providing support in every possible aspect.

I would like to take this opportunity to express my gratitude to my friends for their support and their presence in this wonderful journey, especially Valerie Gono, who saved me from the writing crisis and inspired me with a novel perspective of the world. Li Ji's valuable advice provided me enormous support and encouragement. I would like to express my gratitude to one and all, who directly or indirectly, helped and supported me during this adventure.

Abstract

Comparative Analysis of Lost Circulation Material Particle Size and Degradation in Drilling Fluids

Lin Yang, M.S.E

The University of Texas at Austin, 2015

Supervisor: Eric van Oort, Arthur Hale

Lost Circulation Materials (LCM) are used to plug natural and induced fractures to minimize drilling fluid loss to formations. Various LCMs are available in field application, such as calcium carbonate and graphite. Design of the particle size distribution is crucial to successfully mitigate loss circulation. It is common industry practice to rely on the particle size distribution as specified by the product data sheet when designing lost circulation pills.

During mud circulation, there are several instances where LCMs are exposed to high shear rates, such as during fluid mixing at the hopper, going through mud pumps, and exiting through the bit nozzles. Using sensitive focused beam reflectance measurement (FBRM) techniques, reliable laser diffraction and sophisticated image analysis, we have found that size degradation of calcium carbonate and graphite under such shearing conditions occurs at a lower shearing rate - and to a much larger extent - than previously assumed. This, then, calls into question the effectiveness of calcium carbonate and graphite

for LCM applications that rely on size maintenance for effective bridging purposes.. Based on the experimental results, the field personnel can take size degradation effects into account and compensates accordingly.

Unexpectedly, particle measurements from sieve analysis, FBRM, laser diffraction and image analysis are quantitatively different. This can be attributed to the various definitions of particle diameters and the limitation of each techniques. Image analysis provides the most accurate particle sizing information but the reproducibility of the corresponding equipment is questionable. Laser diffraction is fast and reliable but will be affected by the sampling method and the degree of dispersion. FBRM requires no dilution to the sample, but provides chord length measurement which is very different from the equivalent spherical diameter (the prevailing diameter definition).

In this study, we will show the size degradation results of calcium carbonate and graphite, and the detailed evaluation of the three commercial particle size analyzers used in the experiments.

Table of Contents

List of Tables

List of Figures

Chapter 1: Introduction

Drilling fluid or drilling mud as it is called in the field, is an important component in the drilling process. Drilling fluid consists of both a continuous phase and a dispersed phase. Usually, the continuous phase is the fluid phase, while the dispersed phase is the particulates distributed in the fluid phase. Based on its continuous phase, drilling fluid is categorized into water-based mud, oil-based/synthetic-based mud and gas (Darley and Gray 1988). The focus of this study is water-based mud. The continuous phase of water based mud can be fresh water, sea water or brine. The solids in water-based mud includes weighting material (which help increase mud density), viscosifiers (which help increase viscosity to suspend solids), fluid loss control agents (which control filtration properties) and lost circulation material (LCM, used to bridge in-situ cracks and induced fractures to minimize mud loss to downhole formation, thus also known as bridging particles). The solids traditionally are divided into three different size categories: 1) colloids (less than 2 microns), which usually serve as viscosifier and fluid loss control agent; 2) silt (2-74 microns), among which barite is the most common and is used as weighting material; 3) sand (50-2000 microns), which helps to bridge large pores in the formation (Darley and Gray 1988; ASME, Growcock, and Harvey 2005).

The functions of drilling fluid include, but are not limited to, circulating cuttings out of the wellbore, providing primary pressure control and helping to maintain a stable wellbore (Darley and Gray 1988). Pressure control is provided through the hydrostatic mud column. The drilling fluid fills up the borehole during drilling, and is in contact with the formation. In most cases, the pressure provided by the mud column is larger than the formation pore pressure to prevent the influx of formation fluids. The formation pore pressure is exerted by the fluids inside the pores of formation rocks. Due to this differential

pressure, the drilling fluid will invade the formation when drilling through the permeable rocks. Larger particles seal the pores and deposit themselves with the polymer component of the mud on the formation face, forming a filter cake (the term mud cake is used interchangeably in the remainder of this document). Particles smaller than the pore throat size flow with the continuous phase of drilling fluid (also known as filtrate), passing through the filter cake and into the formation. These small particles will deposite inside the formation, forming an internal filter cake in near wellbore formation. (Ferguson and Klotz 1954).

Problems with the filtration of drilling fluids can cause many problems in the drilling process. Thick, poor quality mud cake may lead to differential sticking. The internal filter cake formed by small particles can block the flow conduit within the pores, thus decreasing the formation permeability (fluid flow capability). This is known as formation damage, which decreases wellbore productivity (Jiao and Sharma 1994). The filtrate also changes the near-wellbore fluid saturation profile, thereby affecting electrical resistivity well log interpretation (Ferguson and Klotz 1954).

When the mud pressure exceeds the formation fracture gradient, fractures are introduced or reopened in the formation. The drilling fluid will leak into the formation through induced fractures and the amount of loss varies according to the size of the fractures. This phenomenon is called lost circulation. Lost circulation often occurs in zones that are high permeability, fractured (both induced and naturally occurring), vuggy or cavernous. The massive loss of drilling fluid can cause various drilling problems, thus increasing drilling non-productive time and cost. This also leads to improper removal of cuttings out of the wellbore, which causes stuck pipe. The decrease in mud level lowers the hydrostatic pressure, which can cause influx of formation fluid. There may even be a

possibility of well control incidents and loss of life if adequate remediation is not applied on time.

LCMs are introduced to drilling fluid system to increase the number of bridging solids and change the particle size distribution. These larger LCM particles are expected to bridge the pores and fractures, which could not be sealed by other components in the mud (White 1956). Optimal selection of LCMs can help minimize formation damage (Abrams 1977), reduce filtrate loss (Dick et al. 2000) and mitigate lost circulation. Large particles bridging pores also prevent further invasion from smaller particles. Filter cake builds up as the particles accumulate on the surface of formation rocks. Ideally, filter cake should be relatively thin with low permeability, preventing invasion of filtrate. Pore sizes vary from formation to formation, therefore the particle size design should be tailored to the formation drilled. There is a variety of guidelines available in the industry on how to determine the ideal particle size distribution (PSD) of LCM for different types of formation (Abrams 1977; Gatlin and Nemir 1961; Smith et al. 1996; Dick et al. 2000; Vickers et al. 2006).

It should also be pointed out that LCM experiences shear degradation under downhole conditions (Scott et al. 2012). Due to the fragility and erosion of bridging material, a higher-than-expected quantity is generally required to mitigate the loss of circulation. It is therefore important to develop a thorough understanding of bridging material, especially with regards to its initial size distribution and its shear resistance. Thus, a study was carried out to characterize the shear degradation behavior of LCMs. Moreover, this study was used to quantitatively assess the accuracy of different measurement techniques and devices to characterize changes in PSD.

Historically, sieve analysis has been used to determine the particle size in drilling fluids. However, manual sieve manipulation is time consuming and human error has a noteworthy impact on the results. Besides sieve analysis, a variety of particle sizing

techniques are available. Three different particle size analyzers (PSAs) were used in the shear degradation experiments reported here:

- Malvern Mastersizer 2000,
- Canty Drilling Mud Particle Size Analyzer,
- Mettler Toledo ParticleTrack G400.

Measurements from sieve analysis were obtained and used as a reference. By comparing the results from various particle sizing techniques, the extent of shear degradation was determined. Moreover, the merits and drawback of different PSA techniques was analyzed. It should be noted that PSAs were not only evaluated for their accuracy of measurement, but also by the ease of their operation and the possibility of being used in a largely automated system in actual field drilling applications.

This thesis examines the shear resistance of popular LCMs (specifically calcium carbonate and graphite) using shear degradation experiments while evaluating three commercial analyzers.

Chapter 2 reviews the particle bridging guidelines, common LCMs and previous shear degradation experiments.

Chapter 3 explains the working principles of all three PSAs used in the experiments, including their schematics. The standard shear degradation experiment procedure is described in details at the end of the chapter.

Chapter 4 presents the experimental data and a discussion of the results. Conclusions will be presented regarding the shear degradation behavior of common LCM particles, as well as the measurement characteristics of the particle size analyzes methods that were used.

Chapter 5 concludes the thesis and provides suggestions on future work.

Chapter 2: Literature Review

2.1 Lost Circulation Materials

Lost Circulation Materials (LCMs) are commonly used to plug pores or fractures in downhole formations. They could be used to reduce filtration, minimize formation damage and to prevent or mitigate lost circulation to formation (Cargnel and Luzardo 1999). They are often used in large volumes, thus warranting the use of inexpensive and readily accessible materials. Common LCMs include calcium carbonate, ground peanut shells, and mica, to name a few. A list of common LCMs is shown in Table 2-1. LCMs are usually classified by their shapes into flaky, granular and fibrous materials (Darley and Gray 1988). Sometimes, materials of different shape are mixed together to create a mixed-shape blend (White 1956).

Table 2- 1 LCM categorized in various shapes (Darley and Gray 1988)

Flaky	**Granular**	**Fibrous**
Cellophane	Calcium carbonate	Asbestos
Cotton seed hulls	Coal	Bagasse
Mica	Diatomaceous earth	Flax shives
Vermiculite	Nut shells: Almond, Pecan, Walnut	Hog hair
	Olive pits	Leather
	Perlite	Mineral wool
	Salt (only in saturated solutions)	Paper
	Synthetic resins	Rubber tires
		Wood: Bark, Shavings, Shreds (fibers)

In this research study, calcium carbonate and graphite LCMs are studied in shear degradation experiments. Calcium carbonate is a widely used LCM, especially in drilling and completion fluids. The advantages of calcium carbonate include its availability in various size ranges for different types of formation, the granular shape which bridges irregular pores effectively, and its solubility in acid which allows it to be removed from reservoir rock during its stimulation (Mahajan and Barron 1980).

Graphite is a resilient, dual composition carbon-based material. Graphite is largely inert and does not adversely affect drilling fluid properties. Graphite has a higher flexibility compared to the other LCMs. It can enter pores easier and deeper, forming an internal seal to prevent further invasion of filtrate. It is also compressible, with the effects of compression under pressure being reversible, which indicates that it could be very responsive to the change in well pressure. As the pressure increases, the particle would be compressed instead of being crushed inside a fracture, thereby maintaining its integrity. As production progresses and the pressure is released, the particle could expand to hold a firm seal in place (Goud and Joseph 2006).

Glass microspheres are used as a reference material in the experiments for the following reasons. Firstly, it is more shear resistant than calcium carbonate and graphite, with a hardness of 6 on Mohs hardness scale (Gordon 2000), while the hardness values are 3 for calcium carbonate (Lide 2005) and 1 for graphite (Cowlard and Lewis 1967) . Secondly, the spherical shape of glass microsphere minimizes the difference in measurements across different particle sizing techniques. Lastly, glass microspheres are inert and they do not react with other components in the drilling fluid.

It is believed that the PSD is the key factor in designing an effective LCM pill (He and Stephens 2011; Mohamed 2011; Mahajan and Barron 1980). In existing literature,

several guidelines are provided for LCMs selection based on particle size. These guidelines are described in the following section.

2.2 PARTICLE SIZE SELECTION GUIDELINES

Abram proposed the "$^1/_3$rd rule" for optimizing the particle size selection of LCMs in 1977. The bridging particles' median particle size (D50) should be at least $^1/_3$rd of the median pore size. Besides that, the concentration of the LCM in the drilling fluid must be at least 5 vol% (Abrams 1977).

Gatlin proposed the application of a maximum density mixture to provide a better plugging effect. The formulation of the mixture is based on Furnas' method, which described how to achieve maximum possible density of packed of solids (Gatlin and Nemir 1961). This method is based on the continuous gradation of sieves. In this method, the ratio between the amount of each size and that of smaller size is defined as

$$r = \frac{1}{\varphi^{\frac{n}{m}}}$$

where r is the ratio between the quantity of successive sizes, φ is the porosity of the bed composed of one screen-size material, n is one less than the number of component sizes obtained from the ordinate of Figure 2-2 and m is one less than the number of the sieve used. K in Figure 2-2 is the ratio between the smallest particle diameter and the largest particle diameter.

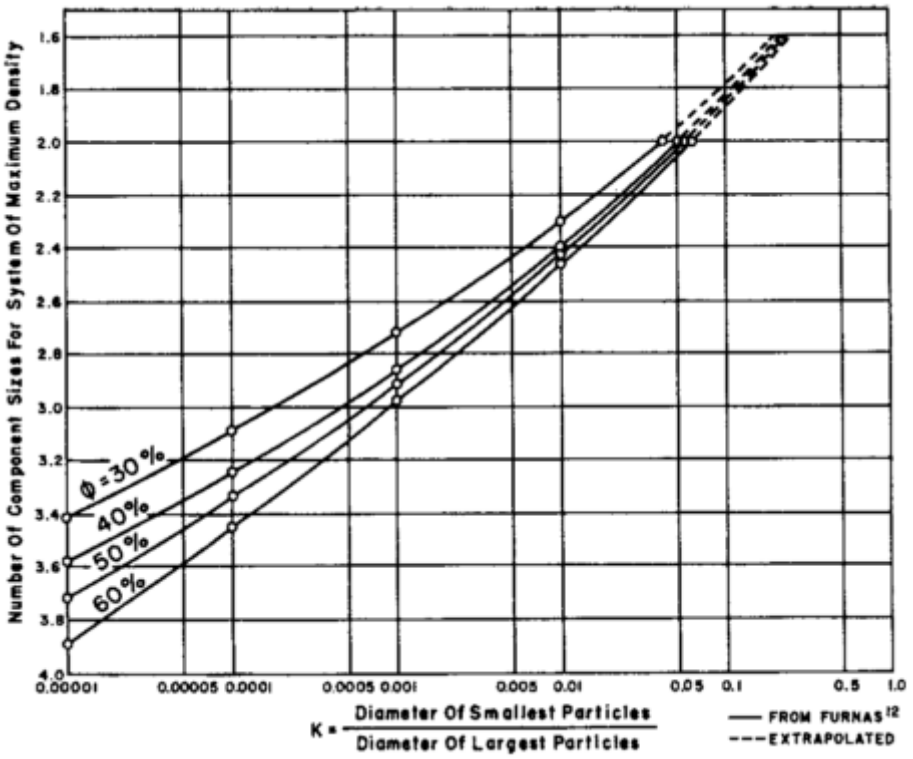

Figure 2- 1 Relation between the size ratio and the number of component size for systems of maximum density (Gatlin and Nemir 1961)

By applying the maximum density theory, it was found that the spurt loss* of bentonite mud in the filter press test was reduced. However, it did not change the volume of filtration along the linear portion of the filtration curve (Gatlin and Nemir 1961).

Smith investigated the proper PSD for application on porous quartz arenite sandstone. He emphasized the importance of D90 (the size of the particle which is larger than the other 90% particles in the system) over D50, which is the only parameter used in

* The initial loss of the drilling fluid to the formation before a proper filter cake is built up on the face of the formation

the $^1/_3{}^{rd}$ rule. Especially in the formation with large pores, it is important to ensure that the particles beyond D90 are large enough to bridge the large pores.

In 2000, Dick proposed the ideal packing theory (IPT) for particle selections. IPT is based on construction of an optimum target line by following a $D^{\frac{1}{2}}$ rule. In a Cartesian graph, the y axis represents cumulative volume percentage while the x axis represents the square root of pore size diameters. By connecting the origin and the square root of the formation's largest pore size diameter on the graph, the target line is formed. This target line is the suggested PSD for the LCM. Minimized filtrate loss and formation damage are achieved by the drilling fluid following IPT according to Dick's documented field trial experiences.

In 2006, Vickers built his criteria based on Abram and Barkman and Davidson's work. Vickers criteria stated that the D90 of the LCM should be equal to the largest pore throat of the formation; D75 should be smaller than two third of the pore throats; D50 should be around the size of one third of the mean pore throat; D25 should be around the size of one seventh of the mean pore throat; and D10 should be bigger than the smallest pore throat. This five-point matching provides precise guidelines for optimal particle size selection (Vickers et al. 2006).

Besides PSD, it is stated in the particle selection guidelines that pore size distribution should be determined, or at least estimated. There are several methods available to measure or calculate representative pore size distribution. If core samples are acquired, lab investigation can be done using one of the four methods below (He and Stephens 2011):

- thin section analysis,
- mercury injection,
- scanning electron microscopy (SEM),
- micro-CT,

If available, a nuclear magnetic resonance (NMR) log could provide the pore size distribution. When a core sample is not available, core and logging data from the nearby areas or geo-statistical models could provide an insight into the pore size distribution.

Thin section analysis, SEM and micro-CT utilize microscopy techniques. They all provide a visualization of the pore structure and enable geologists to characterize pore systems, such as pore shapes and connectivity. Thin section analysis and SEM only provide two-dimensional information of pore systems; however, micro-CT generates three-dimensional information. Undoubtedly, the cost of micro-CT is much more expensive than that of the other methods. Mercury injection method is good at capturing small pores, but might miss larger pores (He and Stephens 2011).

Gas adsorption can provide fast and easy-to-interpret pore size measurements, but there are limitations. Burdine et al. expressed reservations about gas absorption experimental results. They believed that the validity of the assumptions about the thickness and uniformity of absorbed layer is questionable (Burdine, Gournay, and Reichertz 1950). Groen et al. explained the limitation of the interpretation by stating that "major limitations of these models are the non-allowance for network effects and a poor description of the geometrical and energetic effects of the pore and pore wall" (Groen, Peffer, and Pérez-

Ramírez 2003). Fundamental understanding of the model and phenomena are required for a reasonable interpretation of any adsorption data.

Pore size distribution of the formation drilled is clearly an important variable and was considered explicitly in this study.

2.3 Shear Degradation of Lost Circulation Materials

Smith pointed out that the attrition of bridging material is inevitable. The attrition effect in water-based mud was found to be larger than that in oil-based mud. According to his field results, a significant decrease in the D90 of the samples was observed (Smith et al. 1996).

In 2012, Scott investigated the size degradation of various LCMs (walnut hull, pecan hull, graphitic material and ground marble) for 5-, 10- and 15-minutes of shearing time. OFITE mixer (spindle type, refer to Figure 2-2) was used to create low-shear environment and Silverson High-Shear Mixer (Figure 2-3) was used to apply high shear in the experiments. The paper concluded that 250-600 microns ground marble degrades rapidly and almost completely by using the Silverson High-Shear Mixer and experienced less but noticeable degradation with the OFITE Mixer. Walnut hull, pecan hull and graphitic materials were more shear resistant than ground marble, especially in range of 100-600 microns under high shear impact applied by Silverson. Based on his lab results, it was also found that smaller ground marble particles experienced less size degradation (Scott et al. 2012).

However, the shear degradation results are not consistent between low shear and high shear conditions. For instance, the 250-600 microns ground marble experienced the most significant size reduction under high shear impact, but the pecan hull of the similar size range degraded the most under low shear impact. Moreover, Scott used the amount of

material retained on the sieve after shearing to determine the percentage of the degradation. This appears to be a relative rough estimate for the degree of size degradation. Even though the hypothesis that "the smaller the original size of bridging particles is, the lesser the degradation they will undergo" is true for ground marble, it does not hold for other bridging materials (walnut hull and graphitic material).

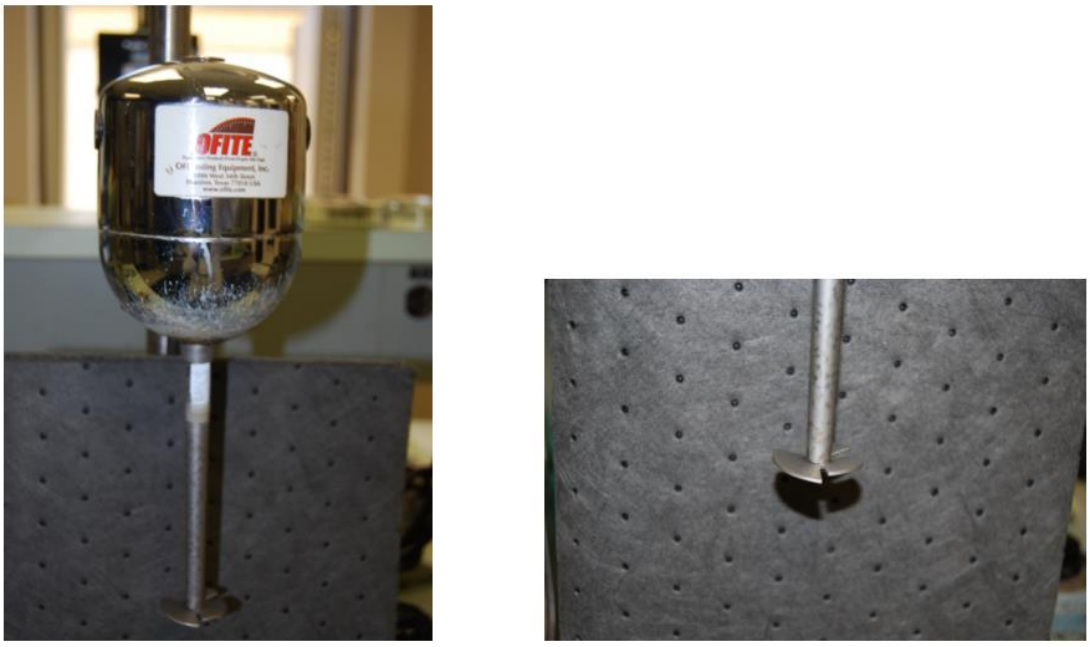

Figure 2- 2 (a) Spindle type mixer; (b) Spilt mixing head of the mixer (OFITE model included in the pictures) (Scott et al. 2012)

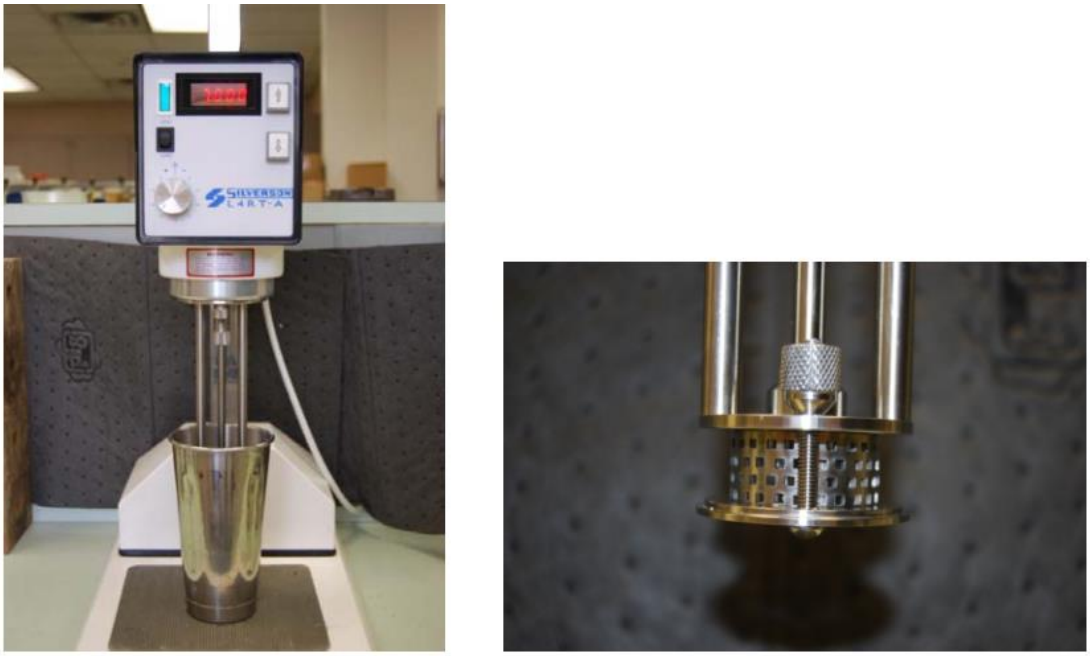

Figure 2- 3 (a) Silverson high-shear mixer; (b) Square-hole high-shear mixing head of the mixer (Scott et al. 2012)

Later in 2013, Kumar et al. conducted a systematic study over the design of bridging material, including an accurate definition of PSD and the consideration of the particle attrition. Kumar applied shear with Silverson high-shear mixer, but used a different mixing head – the general purpose disintegrating head (Figure 2-4). They believed that the laser diffraction technique is less accurate with particle bigger than 100μm, thus sieves were used to measure the particle size. Image analysis was also use to provide visual verification of the material shape (Kumar et al. 2013).

Figure 2- 4 General purpose disintegrating head (Kumar et al. 2013)

Kumar et al. introduced a new parameter to define the degree of size degradation, attrition resistance.

$$R_a = 1 - \left(\frac{D_{to} - D_{t30}}{D_{to}}\right)$$

where D_{to} represents the D_{90} of the original particles and D_{t30} refers to the D_{90} of the particles after shearing. The experiments were designed to investigate the effect of six parameters on particle attrition, which include attrition time, fluid viscosity, shear rate, particle concentration, initial particle size and material type. The effect of attrition time, fluid viscosity, shear rate and particle concentration was studied with calcium carbonate. It was found that longer attrition time, lower fluid viscosity and higher shear rate led to an increase in size degradation of calcium carbonate. But particle concentration did not seem to have any significant effect on size degradation of calcium carbonate (Kumar et al. 2013).

Graphitic carbon and walnut based products were introduced for the comparison of different materials. Impressively, graphitic carbon and walnut based products were much

more shear resistant than calcium carbonate. Calcium carbonate showed a positive trend of increasing particle attrition with increasing initial particle size.

The field study discussed in the Kumar paper showed a significant change in the PSD of a water-based mud after only a few cycles, which highlighted the need to employ regular and precise onsite monitoring of PSD. Overall, the paper clearly proved the fragility of calcium carbonate and the impact of various parameters on particle attrition.

Though three different particle size measuring techniques are included, the paper did not provide any data to support the choice of sieve analysis over laser diffraction. Extensive experiments were conducted with calcium carbonate, but only few with the other materials to conclude the extraordinary shear resistance of graphitic carbon and nut based product.

While both Scott and Kumar approached the problem experimentally, Valsecchi's work provided a new angle for understanding the size degradation of bridging materials by analyzing the dynamic behaviors of the downhole flow. The paper classified the interactions occurred during the drilling cycle into three categories, namely the interactions of bridging solids with the fluid, the interaction between bridging solids and the interaction of bridging solids with the machine boundaries, such as the bit, drill pipe walls, etc. (Valsecchi 2014). The latter two mechanisms contributed the most to the degradation of bridging particles.

The interaction between bridging solids dominated the flow in the drill pipe, drill collar and possibly the annulus. The impact of this mechanism is indicated by the Reynolds number. As Reynolds number increases, more turbulent flow conditions lead to more collisions between solids resulting in severe size degradation. The interaction between bridging solids and walls in the sections of changing flow path, for example, the flow through nozzles, is quantified by the Archimedes number. As stated in the paper (Valsecchi

2014), “The likelihood of collision against a solid boundary increases with the particle Archimedes number and, consequently, so does the degradation rate”.

By understanding the two dominating mechanisms, one could select suitable LCMs targeted for different sections. For instance, Archimedes number is affected by the particle size and the density difference between the particles and drilling fluid, thus a mud engineer could select the bridging particle which helps reduce the Archimedes number.

Valsecchi also pointed out that the interaction between particles and walls contributed the most to size degradation. Previous lab experiments with counter top mixer do not properly simulate this mechanism. The shear that could be applied under lab conditions is much less than that of a drill bit.

Combining the theoretical and experimental understanding of shear degradation, it is important to choose appropriate particle size measurement techniques that can be used in both laboratory and field environments. In our experiment, the size degradation of calcium carbonate and graphite were quantified, and compared with those published by Scott and Kumar.

2.4 Particle Size Measurements

To determine the best suitable particle sizing technique, a fundamental understanding of particle size is necessary. In this section, the concept of particle size is discussed and various particle size characterization techniques are presented.

2.4.1 Particle Size Definition

The size of a spherical particle is obvious, as it is straightforwardly characterized by the diameter of the sphere. For rectangular, cubic or other particles with a common shape, particle size can be easily explained. When it comes to particles with irregular shape, the case is different. This is why the concept of derived diameter is important.

As stated in Allen's book, "Derived diameters are determined by measuring size-dependent properties of particles and relating them to single linear dimensions". The most popular one is the equivalent spherical diameter (Allen 1996). The size of an irregularly shaped particle usually depends on the particle sizing tools used. For example, if a laser diffraction tool is used, the diffracted light intensity is recorded which relates to the volume of the particulate. Assuming that there exists a sphere of that volume, the diameter of that sphere is calculated. This equivalent spherical diameter (Fig 2-5) is recorded as the size of this specific particle. The size-dependent property could be volume, weight, sedimentation rate, etc.

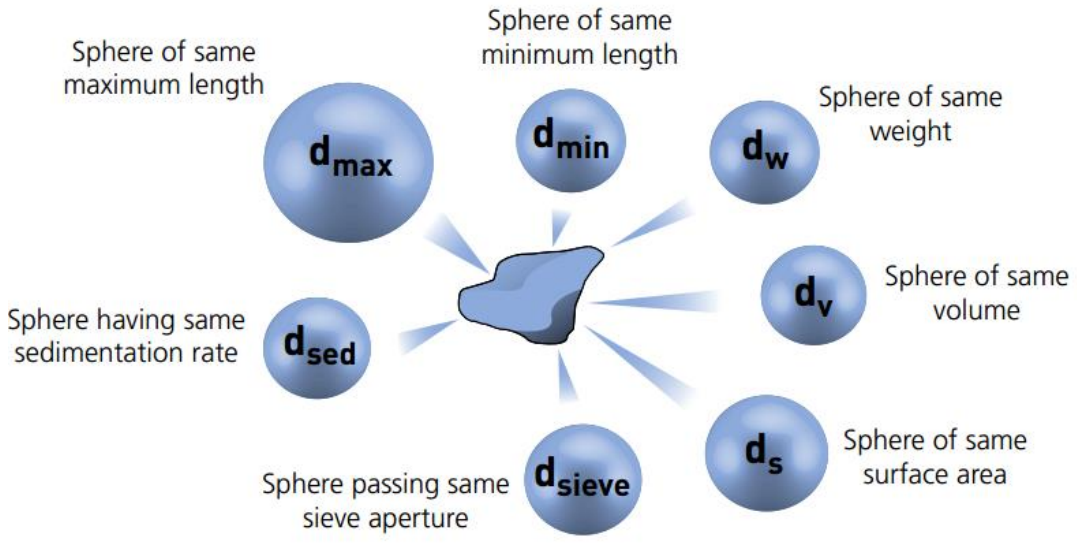

Figure 2- 5 Concept of equivalent spherical diameter (Malvern Instruments Ltd 2012)

Besides the widely used equivalent spherical diameter, there exist other important particle diameter definitions, such as sieve diameter, Martin's diameter, Feret's diameter and projected area diameter. These definitions along with the relevant formulas are listed in Table 2-2.

Table 2- 2 Definitions of particle diameters (Allen 1996)

Symbol	Diameter	Definition	Formula
d_v	Volume	Diameter of a sphere having the same volume (V) as the particle	$V = \frac{\pi}{6} d_v^3$
d_s	Surface	Diameter of a sphere having the same external surface area (S) as the particle	$S = \pi d_s^2$
d_{sv}	Surface-volume (Sauter)	Diameter of a sphere having the same ratio of external surface area to volume as the particle	$d_{sv} = (d_v^3/d_s^2)$
d_d	Drag	Diameter of a sphere having the same resistance to motion as the particle in a fluid of the same viscosity and at the same velocity (d_d approaches d_s when Re is small)	$F_D = 3\pi d_d \eta v$ *
d_f	Free-Falling	Diameter of a sphere having the same free-falling speed as a particle of the same density in a fluid of the same density and viscosity	

* F_D is the drag force, η is the fluid viscosity and v is the velocity of the object.

Table 2- 2 Definitions of particle diameters (Allen 1996)

Continued

d_{St}	Stokes	Free-falling diameter in the laminar flow region	$d_{St} = \sqrt{d_v^3/d_d}$
d_a	Projected area	Diameter of a circle having the same projected area as the particle in stable orientation	
d_p	Projected area	Diameter of a circle having the same projected area as the particle in random orientation [for convex particles, mean value for all orientations $d_p = d_s$]	
d_c	Perimeter	Diameter of a circle having the same perimeter (P) as the projected outline of the particle	$P = \pi d_c$
d_A	Sieve	Width of the minimum square aperture through which the particle will pass	
$^*d_F$	Feret	The distance between pairs of parallel tangents to the projected outline of the particle in some fixed direction	
$^*d_M$	Martin	Chord length, parallel to some fixed direction, which divides the particle projected outline into two equal areas	
$^*d_R$	Unrolled	Chord length through the centroid of the particle outline	

* statistical diameters, often defined in terms of the mean value for a particular particle

2.4.2 Particle Size Characterization Techniques

Traditionally, there are three particle size determination methods utilized in the oilfield: the API sand content test, sieve analysis, and the sedimentation method (Darley and Gray 1988).

An API sand content test kit includes a glass measuring tube, a sieve and a funnel. The objective of the test is to determine the volume percentage of the particles which are bigger than 74 μm (American Petroleum Institute. Production Department 1990).

The sieve analysis is conducted by shaking and vibrating particles through a stack of sieves. The openings of neighboring sieves determine the size of particles retained on the sieve with smaller aperture. Thus, the resulting PSD is discretized. Sieve analysis usually involves human error and is time consuming due to the manual labor involved.

The Sedimentation Method is usually applied to sub-sieve size particle (<37 μm), and is based on Stokes' Law. Given the settling velocity of particles, one can calculate the diameter of particles by assuming that only spherical particles are present. Sedimentation performs better with a narrow range of particle sizes. It usually takes a long time to finish one test, especially for smaller particles.

Laser diffraction is a trending particle sizing technique due to its fast operation and reliable results. The laser light is passed through a sample cell filled with dispersed particles. The particles has to be dispersed in water or other solvent (air, alcohol, etc.). Particles diffract the incident light at various angles based on the diameter of particles. The detector then captures the intensity of the diffracted light. The intensity pattern is then correlated with the PSD. The output from laser diffraction is expressed as equivalent

spherical diameters. The concentration of solids should be limited to allow light to pass through the sample.

Focused beam reflectance measurement (FBRM) also uses laser to determine particle size. In FBRM, the laser light is highly focused. As the laser beam passes through the sample, the back-scattered light from the particles will change accordingly. The system can identify how long the particle is in contact with the laser beam based on the return signal (Allen 2003). The output is based on the chord length of particles, which is quite different from those of other techniques by definition: the chord length of a particle is a line segment connecting any two points on the boundary of the particle.

Dynamic light scattering (DLS), also known as photon correlation spectroscopy (PCS), is typically used for sub-micron particles. The scattering light coupled with the Brownian motion will yield a speckle pattern, which is the results of the destructive and constructive interferences. This fluctuation of the diffraction is related to the diffusion coefficient, which can be used to calculate particle size (Allen 2003). The resolution of this technique is relative low and the sample has to be diluted to avoid multi-scattering effect before measuring.

Electronic sensing zone, also known as the Coulter counter, is another technique used to measure particle size. A liquid containing the particles is passed through an orifice with electrolytes at either end of the orifice. The electrical impedance of the liquid will change accordingly as the particles pass the orifice, and is used to calculate the corresponding particle size (Allen 2003). This technique is only applicable for water-based mud. In order to measure oil-based mud, the particles have to be extracted from oil and re-dispersed in the water to be measured (Darley and Gray 1988).

Optical microscopy and electron microscopy can both be used to determine particle size. Since the method has to be compatible with analyzing a drilling fluid, optical

microscopy will be more useful. Electron microscopy usually has a stricter requirement towards the environment. Optical microscopy, known as image analysis, usually has a lower limit of 0.8 μm. The camera captures a visual image of the sample with dispersed particles and determines the particle size with advanced imaging algorithm. Image analysis is the only technique that can report multiple values about a particle, giving its advantage when describing irregular particles (HORIBA Instruments Inc. 2014). It can report a particle's longest and shortest diameter, perimeter, projected area, equivalent spherical diameter, aspect ratio and circularity. However, due to its small depth of focus, it has difficulty in capturing all the particles from a sample with wider PSD, and generally requires dilution in order to deal with more opaque fluids.

Ultrasonic extinction utilizes sound waves instead of light, which could be used to measure particle size of a highly concentrated fluid (Karimi 2013). A complicated mathematical model developed by Allegra-Hawley can be used to predict the attenuation of an acoustic wave transmitted through a sample as a result of frequency, solids concentration and size distribution (Allen 2003). This enables the possibility of using ultrasonic extinction to develop an on-line particle size analyzer (OPUS) (Sympatec System Particle Technology 2015). The complexity of this method is directly related to its advanced mathematical model. Some flow properties are required for both dispersed and solvent phases. For higher concentrations (5 vol% to 10 vol%), the assumption of a single scattering condition is not valid and the effect of multiple scatterings has to be included in the model. At even higher concentrations, the scattering model will lose its validity, and empirical correlations have to be coupled into the model.

2.4.3 Particle Size Distribution and Statistics

The most common PSD is volume-weighted. However, there are other weighted distributions, such as number-weighted and mass-weighted. How the distribution is weighted usually depends on the particle sizing technique applied.

Number-weighted distribution is obtained when the technique counts individual particles. The image analysis and FBRM methods discussed before produce number-weighted distributions, but these can be converted to other weighted distribution.

Volume-weighted distribution is usually obtained by laser diffraction. Mass-weighted distribution are given by sieve analysis. However, when the density of particles is consistent, it can be easily converted to a volume-weighted distribution.

In order to compare the PSD from different techniques, the conversion from one weighted distribution to another weighted distribution is required. The assumptions made during the conversion and the change in statistics has to be taken into consideration during the comparison. For instance, when converting from a number-weighted distribution to a volume-weighted distribution, the volume-weighted distribution will have higher values at the coarser end (see Figure 2-6).

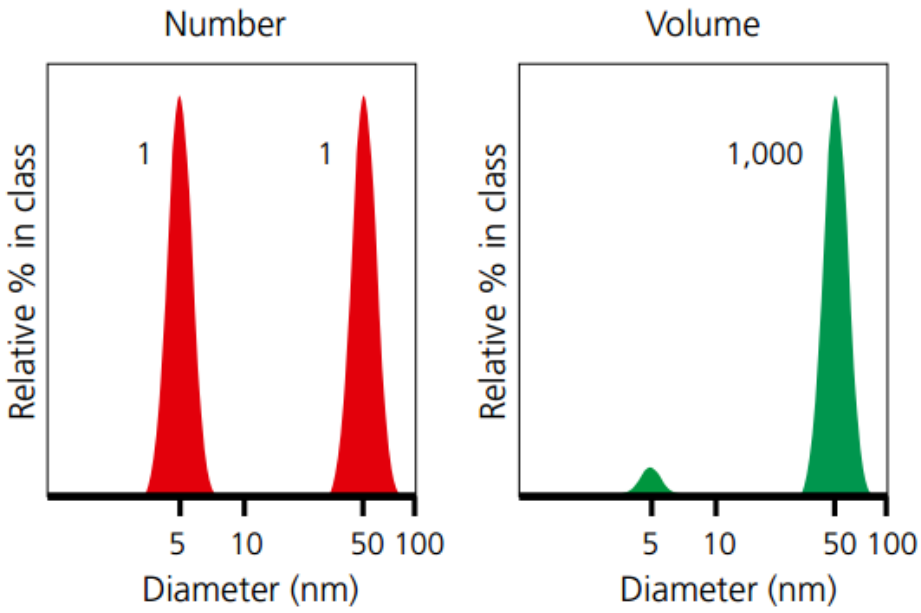

Figure 2- 6 Number and volume weighted distribution of same sample (Malvern Instruments Ltd 2012)

The most commonly used metrics to characterize PSD's include mean and median. Mean is the average particle size of the sample, while the median is the midpoint when arranging all the particle sizes in the sample from highest to lowest. D values can be used to describe a PSD. Three common percentiles (D10, D50 and D90) are often reported to give a general idea regarding the complete PSD. Figure 2-8 shows common percentiles used in the volume-weighted distributions. The x axis in the figure represents particle size and the y axis represents cumulative volumetric percentage. Dv0.1 is equivalent to Dv10, while "v" represent volume.

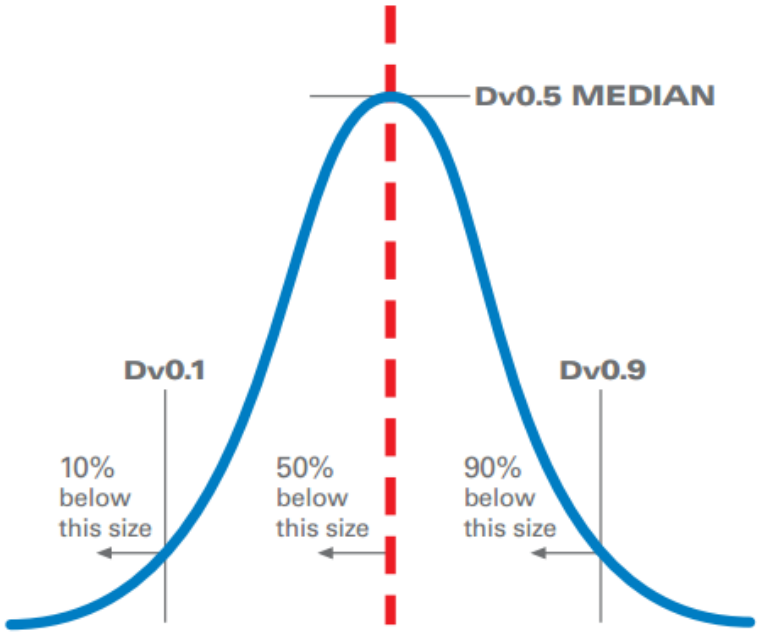

Figure 2- 7 Common percentiles, Dv0.1, Dv0.5 and Dv0.9 (HORIBA Instruments Inc. 2014)

Chapter 3: Equipment and Experimental Procedure

3.1 EQUIPMENT

Chapter 3.1 presents a description of the particle size analyzers (PSAs) used in this study. A good understanding of all PSAs builds the required foundation for analyzing the results obtained from the equipment.

Table 3-1 shows a simple comparison between three PSAs.

Table 3- 1 Comparison of three PSAs

	Malvern Mastersizer 2000	Canty Drilling Mud Particle Size Analyzer	Mettler Toledo ParticleTrack G400
Technique	Laser Diffraction	Image Analysis	FBRM
Size Range	0.02 – 2000 μm	Larger than 1 μm	0.5 – 2000 μm
Measured Particle Size	Equivalent spherical diameter	Minor axis	Chord length
PSD	Volume Weighted	Volume Weighted	Count Weighted
Dilution	Yes	Yes	No

3.1.1 Malvern Mastersizer 2000

Malvern Mastersizer 2000 (Malvern, shown in Figure 3-1) can be used to measure the PSD of samples based on laser light diffraction. This particular equipment is based on the laser diagnostic technique presented by Swithenbank in 1976 (McCave et al. 1986).

Swithenbank and his colleagues stated that the diffraction pattern of a group of droplets is related to the PSD of the droplets. A typical optical setup (Figure 3-2) of Malvern includes a laser light source, a focusing lens, a sample cell and a series of detectors to capture diffracted light produced over a broad range of angles (Kippax 2005). The measurable particle size range is between 0.02 to 2000 μm.

Figure 3- 1 Malvern Mastersizer 2000 (Malvern Instruments Ltd 2015)

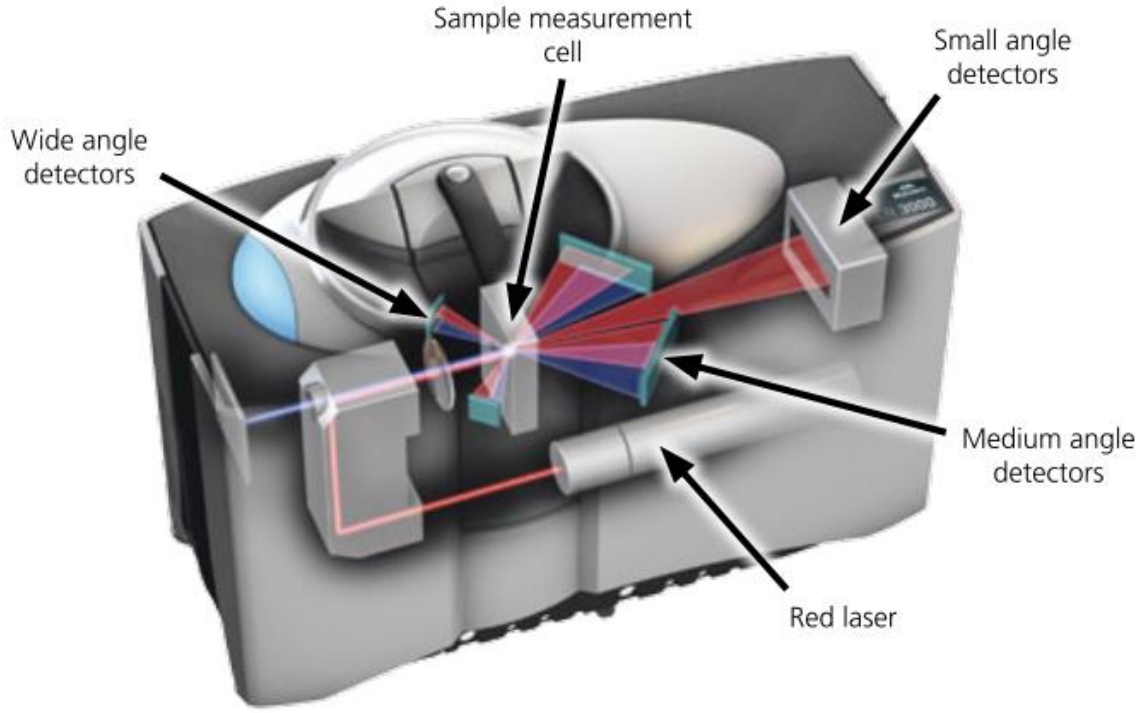

Figure 3- 2 Typical laser diffraction instrument layout (Malvern Instruments Ltd 2012)

Two optical models are commonly used in converting the sample's scattering pattern into a PSD: the Fraunhofer Approximation and the Mie Theory. The Fraunhofer Approximation works better with large particles while the Mie Theory is more accurate with fine particles (Kippax 2005).

The operating procedure of the equipment is as follow. Place 800 cc of deionized water in a standard 1-liter beaker. It serves as the dispersant for measuring water-based mud. The equipment first measures the background (the light intensity pattern of the dispersant), then prompts user to add the sample to the dispersant.

The amount of the sample added depends on the concentration of the particles in the mud. Because the number of particles in the sample should be sufficient for the laser light to diffract on, but not too much as to completely block the laser path. Thus, if the concentration of particles in the drilling fluid is high; the amount of sample added to the dispersant should be smaller and vice versa. This is also indicated by the obscuration (which represents the amount of the light intensity absorbed by the particles) measured by the equipment while the sample is being added to the dispersant. For example, if 30% of light is absorbed as it passes through the sample, the obscuration is 30%. The optimal range of the obscuration is between 10% and 20% as suggested by the company (Malvern Instruments Ltd 2007).

In the sample (wet) dispersion unit (Figure 3-3), the stirrer helps to suspend the heavy material in the fluid. The "dip-in" sample recirculation head connects the reservoir (beaker) to the optic bench. The pump speed was set to 2000 rpm. If the pump speed is too low, it will lead to the settling of solids. If the pump speed is too high, it will introduce gas bubbles into the fluid. The pump circulates the fluid through the measurement area of the optical bench, then it returns the fluid back to the reservoir – the beaker. The dispersion unit can apply sonication to help with the dispersion of samples. However, in our application, sonication was not helpful, and instead of dispersing the particles, more gas bubbles were introduced into the system. Possible breakdown of the particles might also be introduced because of sonication (Beare and Ballard 2013).

Figure 3- 3 Wet dispersion unit for Malvern Mastersizer 2000 (Malvern official website)

The laser beam passes through the fluid and scatters at different angles based on the size of the particles in the system. The light scatters at a smaller angle when it hits large particles, while the light scatters at a larger angle when it is in contact with smaller particles. Multiple detectors in the optical bench capture the scattering pattern, which reflects the PSD of the fluid. The software then compares the scattering pattern with the Mie model. The optical properties (refractive index and absorbent index) are required for the data processing and are listed in Table 3-1. The resulting PSD is volume-weighted. The particle size measured with this technique is the diameter of a sphere with the same volume of the particle.

Table 3- 2 Optical properties of the materials used in this study

Material	Refractive Index	Absorbent Index
Water (Dispersant)	1.33	
Soda Lime Glass	1.513	0.1
Barium Sulfate	1.643	0.1
Calcium Carbonate	1.69	4
Graphite	2.4175	0.5

3.1.2 Canty Drilling Mud Particle Size Analyzer

Canty Drilling Mud Particle Size Analyzer (Canty) is based on image analysis. Image analysis is regarded as the most direct way to obtain particle sizes (Allen 2003). For image analysis technique, there are three essential stages: image capture, image processing, and image analysis (Xu 2002). The illuminated light is provided for a charge-coupled-device (CCD) camera to capture the images of flowing particles (see Figure 3-4). Digital images allows a higher flexibility in computer manipulation, compared to the old days film (Davidson and Abramowitz 1999). Image processing and analysis are achieved with the CantyVisionClient^{TM} software. Users can apply the particle filter to screen out noise in the images. The parameters of the particle filter are usually tailored to a specific system (combination of particle and dispersant). Adjusting the experimental parameters is complicated and often requires the guidance from an experienced user.

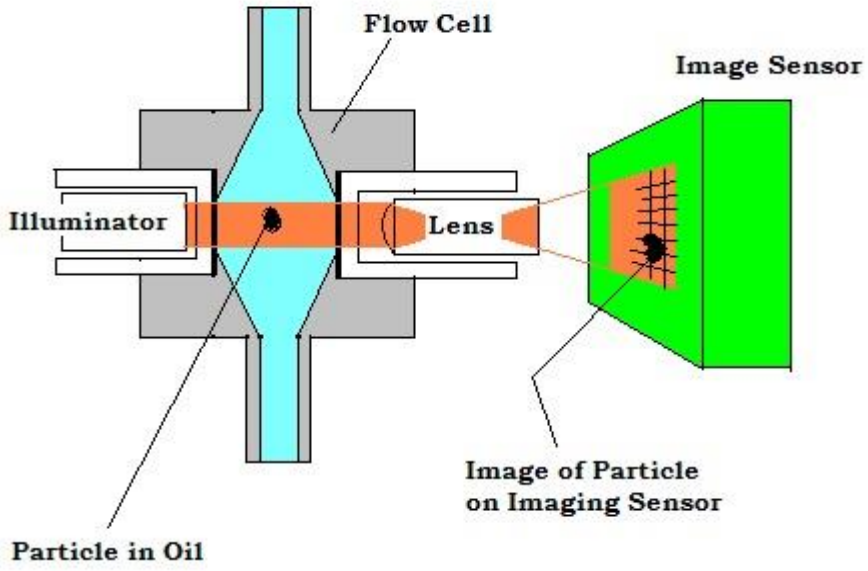

Figure 3- 4 Schematic layout of Canty vision system (Canty 2012)

The measurable range is between 1 μm to approximately 600 μm without making changes to the lens and camera arrangement. Note that equipment does not really have a designated upper limit and that its measurable range depends on the lens installed. This equipment consists of several components (Figure 3-5), including a mixing tank, a stirrer, a reservoir (not shown in Figure 3-5), a pump, a light source, a vision system, a workstation and a waste disposal system (not shown in Figure 3-5).

Figure 3- 5 Lab set-up of Canty Drilling Mud Particle Size Analyzer

The mixing tank on the top of the equipment, along with the stirrer, helps to ensure the homogeneity of the fluid to be measured. The pump draws the base fluid from the reservoir, usually controlled by the auto-dilution function of the software. The vision system and the software are the core of the equipment, providing live images of fluid as and the real-time particle analysis. The waste disposal system takes care of the diluted fluid.

General lab procedure is described as follows. 5-10 cc of drilling fluid is usually required for a representative measurement. As the solid concentration decreases, the

volume of sample should be increased to ensure the representativeness of the sample. The mixing tank is prefilled with 1 liter of base fluid. The drilling fluid formulation determines the base fluid. For example, the base fluid for water based mud is water, while the base fluid for ester oil based mud is that particular ester oil used in the mud. In this study, the base fluid was water. The sample will go through two stages of dilution. The first dilution happens while adding the sample into the mixing tank and mixing until the fluid in the tank becomes homogeneous (usually requires 2 minutes in this study). The fluid flows down along the pipe, and is joined by the water provided by the pump, which is the second dilution. The second dilution is controlled by a software routine called Auto Dilution. Auto Dilution ensures that all the particles in the fluid are well dispersed in the images. Thus, it provides an accurate analysis of the particle sizes. As the fluid goes through the vision system, the live images of flow are shown on the computer. The user could choose to conduct the particle analysis real time which requires a powerful workstation, or to record the video and save it for later analysis.

The software provides more than just PSD. The information it can provide includes, but is not limited to, major (longest) and minor (second longest) axis, aspect ratio, perimeter, projected area, etc. Minor axis is set to be the particle size, in order to be better compared to the sieve analysis results. The output PSD is converted from number-weighted to volume-weighted by default.

If a user chooses to record a video of the measurement, it is easy to relate the abnormal value in particle sizes from the output Excel sheet to the specific particle in a

certain frame on the video. The equipment provides users with visual verification of the particle size and the flexibility of performing data analysis any time after the experiment.

3.1.3 Mettler Toledo ParticleTrack G400

Mettler Toledo ParticleTrack G400 (MT) uses a focused beam reflectance measurement (FBRM) technique, which is "a single particle measurement technique" (Xu 2002). The measurement range is from 0.5 and 2000 μm and the data acquisition rate is 0.5 Hz, which means that a scan is performed every 2 seconds.

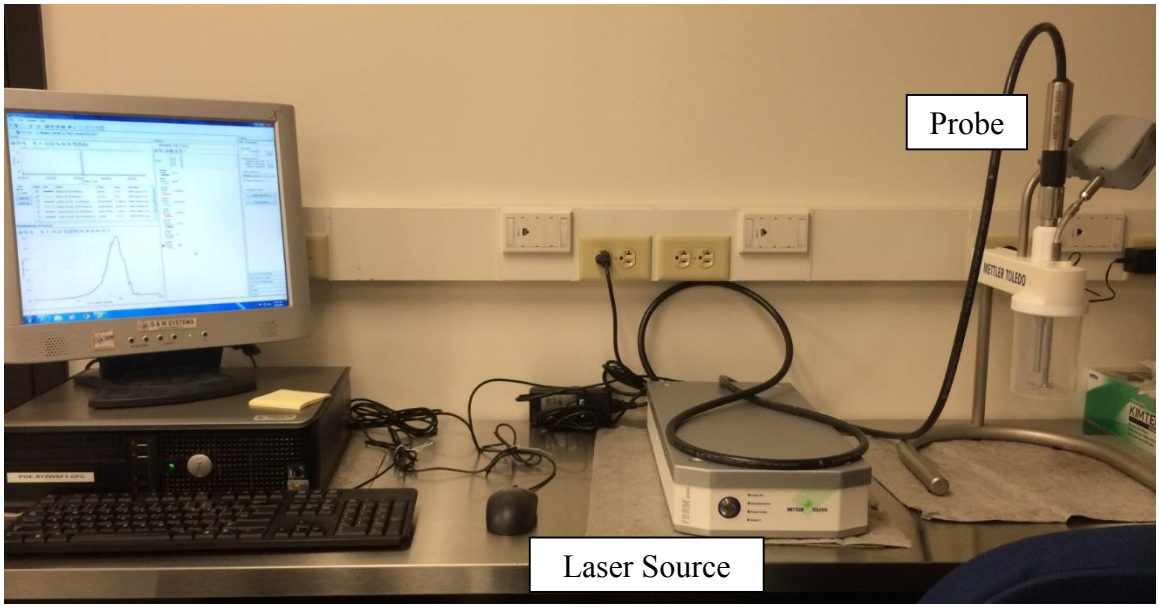

Figure 3- 6 Lab set-up of Mettler Toledo ParticleTrack G400

The major components of the equipment include a probe and a laser source. Figure 3-6 shows the lab set-up with extra beaker and mixer. The measurement procedure is as

follows. Fill the sample to the line in the beaker, approximately 300 cc in volume. No dilution is required for the sample. The probe is immersed in the sample. The measurement is conducted while the overhead mixer is set to 400 rpm. The schematic layout of the probe is shown in Figure 3-7.

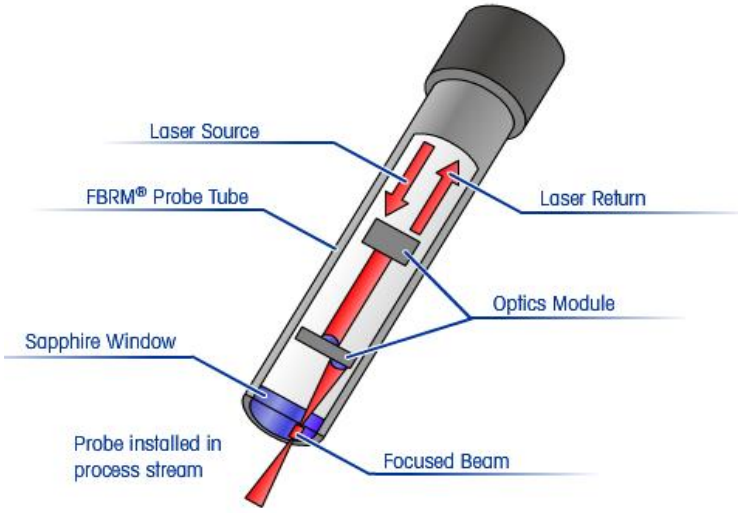

Figure 3- 7 Schematic layout of FBRM probe (Mettler-Toledo International Inc. 2015)

The laser passes through multiple optical modules to form the rotating focused beam. The focused beam scans the surface of the sapphire window. The laser is scattered back as soon as it detects the particle and the detector captures the signal. Combing the rotational speed of the focused beam and the frequency of the signal (Xu 2002), the real-time chord length of particles is acquired and showed on the screen (Figure 3-8). This real-time measurement is presented as a chord length distribution with statistics (eg. mean, number of counts) which are trended over time.

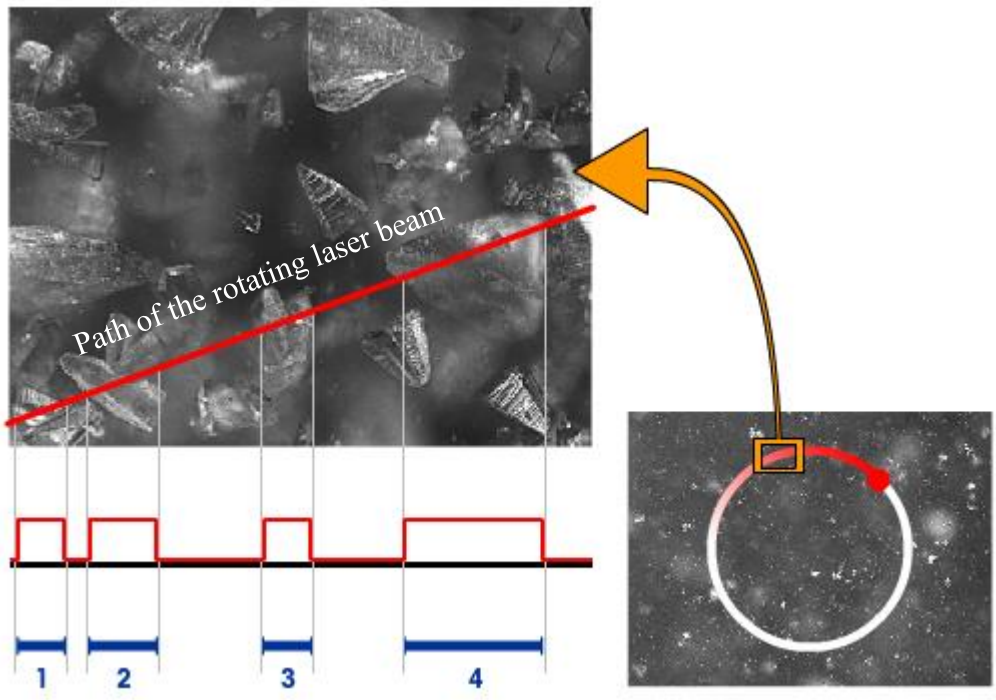

Figure 3- 8 Schematic of how the chord length of particles are measured (Mettler-Toledo International Inc. 2015)

The default chord length distribution is based on particle counts. To compare the results with the results from other PSAs, the number-weighted distribution is converted to a volume-weighted distribution by taking the square of the particle sizes.

In addition to the simple lab set-up shown in Fig 3-6, another, more sophisticated setup (Figure 3-9) was used to create a better flow regime of the sample. It is similar to the set-up recommended for field use. The flow cell was specially designed, so the angle between the probe and the incoming flow is at 45 degree. This is the optimum operating angle for ParticleTrack G400 as suggested by the Mettler-Toledo, its manufacturing

company. The flow loop provides better mixing for fluids, especially in the upward flow section. The particles are more uniformly distributed, thus resulting in a more accurate measurement on PSD.

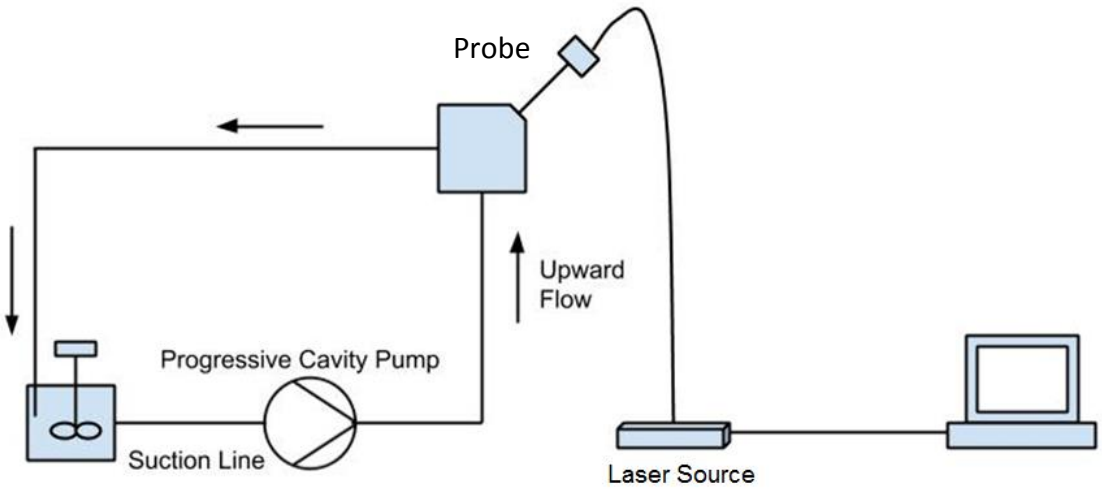

Figure 3- 9 Recommend flow loop set up for ParticleTrack G400

3.1.4 Dry Sieving

Sieving is the classical way of performing particle size analysis, and is still used in the oilfield for cuttings analysis. A stack of sieves is prepared at the beginning of sieving, according to an initial rough estimate of the particle size range. The sieve with the largest opening is located on the top of the stack. The size of the openings decreases from top to the bottom. The receiver pan is located at the bottom of the stack to capture the residue. In order to obtain a representative sample, vigorous shaking is applied to the container for the material to achieve a good sorting of material. The sample size required for a sieve analysis

(Table 3-3) could be determined by the particle density or by the median diameter (Allen 2003).

Table 3- 3 Amount of sample required for a sieve analysis on an 8 inch diameter sieve (Allen 1996)

a) Based on particle density

Density (g/cm3)	Sample weight (g)
1.5	25
1.5 – 3.0	50
3	100

b) Based on median diameter

Median (mm)	Sample weight (g)
>2	500
2-1	200
1-0.5	100
0.50-0.25	75
0.25-0.075	50
<0.075	25

The sieve analysis procedure is as follow. Use the scoop to spread the sample on the top of the sieve stack gently. Start the sieve shaker (Figure 3-9) to apply vibration in intervals. The optimum shaking time was determined by comparing the results from 5-

minutes, 10-minutes and 20-minutes of shaking. A short shaking period would not separate the particle thoroughly to its correct size range, while prolonged sieving might cause the breakages of friable particles. Based on trial and error, it turned out that 10 minutes was an optimal sieve shaking duration, considering the time consumed and the accuracy of results. The smaller particles will pass through the opening of sieve with the aid of vibration and the larger ones will stay on the sieve. It is believed that sieving measures the second largest dimension of the particles (Allen 2003).

After the completion of vibration, the weight of the particles retained on each sieve was measured. The acquired PSD is not continuous, but fractional.

To ensure accuracy, the results of a sieve analysis were determined by taking the average of three tests. The size of different samples was determined from Table 3-3 and the initial size information of the material. For glass microspheres, carbonate fine and graphite fine, the sample size was typically 25 grams. For carbonate regular and graphite regular, the sample size was 50 grams.

Figure 3- 10 Sieve shaker, Ro-Tap Model RX-29-E

3.2 EXPERIMENTAL PROCEDURE - SIZE DEGRADATION EXPERIMENT

The objective of the experiment was to investigate the size degradation of LCM caused by the shear applied through mixing. The experiment was conducted with two grades of calcium carbonate and graphite respectively and glass microspheres. Glass

microspheres were used as the reference material, characterized by the fact that the particle size does not change as the shearing time increases.

The experimental procedure listed below uses glass microspheres as an example. The same procedure is repeated with two grades (fine and regular) of calcium carbonate and graphite.

1. Prepare 1 lab barrel (lab bbl, equivalent to 350 cc) of water-based mud of 1.5 pound per barrel (ppb, equivalent to grams per lab barrel) xanthan gum. Mixing time is 7 minutes for common viscosifiers.
2. Add 10 grams of the glass microspheres into the 1 lab bbl water-based mud while stirring the fluid with spatula slowly with a vortex present.
3. Stir the mud for one minute with a spatula to help disperse the glass microspheres in the fluid.
4. Transfer the mud into a mason jar and label it Sample A, which is the 0-minute-shearing sample.
5. Repeat Step 1 to 3 and followed by applying shear with OFITE Mixer at 8000 rpm for 5 minutes.
6. Transfer the mud into a mason jar and label it as Sample B, which is the 5-minutes-shearing sample.
7. Repeat Step 5 with 10 minutes-, 20 minutes- and 30 minutes -shearing time. Transfer three mud samples into separate mason jars and label them as Sample C, Sample D and Sample E, which are the 10- minutes-, 20-minutes- and 30-minutes-shearing sample.

8. Place all the mason jars in a roller oven. Roll the mason jars for 16 hours at room temperature to eliminate the bubbles in the mud.
9. Take all the samples out of oven after 16 hours and stir it by a spatula for one minute to agitate the mud. Make sure that a full vortex is developed in the mud while stirring.
10. If the glass microspheres are not uniformly distributed in the mud, apply a low shear by Ofite field mixer to help the dispersion. The operator should always exercise caution when using the mixer after completing the rolling and also to prevent further shearing of the particles.
11. Measure the particle size distribution of the mud samples with Malvern Mastersizer 2000, Canty Drilling Mud Particle Size Analyzer and Mettler Toledo ParticleTrack G400.
12. Measure the rheological profile of the mud samples at 120°F. Whenever needed, the operator should stir or mix the mud to help with uniform dispersion of glass microsphere.
13. Repeat step 1-12 for calcium carbonate and graphite.

Chapter 4: Results and Discussion

This chapter presents the experimental results and corresponding analyses. The chapter is ivided into two sections: (1) the evaluation of three commercial PSAs, and (2) the size degradation experiment results. The goal was to identify a suitable PSA for field applications and to investigate the effect of shear intensity on the size degradation of LCMs (namely calcium carbonate and graphite in this study).

4.1 Evaluation of particle size analyzers

As discussed previously in Chapters 2 and 3, the shape of particles affects the output of PSAs. Most PSAs show agreement on the measurement of spherical particles. Thus, glass microsphere are used as a reference material due to their spherical shape.

The evaluation of three commercial available PSAs, namely Canty Drilling Mud Particle Size Analyzer (referred to as Canty), Malvern Mastersizer 2000 (referred to as Malvern) and Mettler Toledo ParticleTrack G400 (referred to a s MT) is conducted by comparing the measurements obtained from each PSA with those obtained using the sieve analysis. As discussed in the previous chapter, results from sieve analysis is considered as a yardstick in the industry. The closer the measurements to the sieve analysis results are, the more accurate the measurements are considered to be. However, sieve analysis is time consuming and is more accurate for larger particles than smaller particles..

Based on the discussion in the following sub sections, Canty produced the best quantitative results as it matched the sieve analysis results the best. Besides that, Canty also provides visual verification for abnormal particle size measurements. Malvern and MT showed a better reproducibility of measurements. Malvern had a well-established

reputation within the industry. In most applications, laser diffraction is the standard go-to particle size measuring technique. Both Canty and Malvern required drilling fluid samples to be diluted before measuring. However, MT does not require dilution, which makes it easier to implement in the rig. In fact, a Mettler Toledo's PSA based on laser diffraction was installed on the Scarabeo 5 rig to monitor solid control processes and sieve shaker failures (Ronaes, Fossdal, and Stock 2012). Among all the three PSAs, however, the MT equipment is also the most sensitive to small changes in particle size.

4.1.1 Glass Microspheres

The vendor used Malvern to measure the PSD of glass microspheres, and provided the measurements as shown in Table 4-1 on the row labeled as literature data.

Table 4- 1 Comparison between the literature data (Cospheric LLC. 2014) and the measurements from sieve analysis, Canty, Malvern and MT for glass microsphere in terms of D10, D50 and D90

	D10, μm	D50, μm	D90, μm
Literature Data	48.0	69.0	83.0
Sieve Analysis	56.8	69.7	84.9
Canty	60.8	71.7	87.8
Malvern	52.2	71.5	98.0
MT	22.4	72.4	121.6

The procedure for the preparation and the measurements of the glass microspheres is described in details in section 3.2, and the same procedure was used for graphite and calcium carbonate.

Figure 4-1 is plotted with three data points, D10, D50 and D90, obtained from each PSA. These numbers (also shown in Table 4-1) describe the average and the range of the sample's particle size. All D50s (or average particle size) agree very well with each other. There is a small discrepancy in D10s and D90s. However, MT's D10 and D90 are much different compared to both the literature data and the sieve analysis results. Since the equipment measures the chord length of particles, this could explain why the measurement has lower D10 even for highly spherical particles. The high D90 may result from the particles overlapping with each other in an undiluted sample measured by MT.

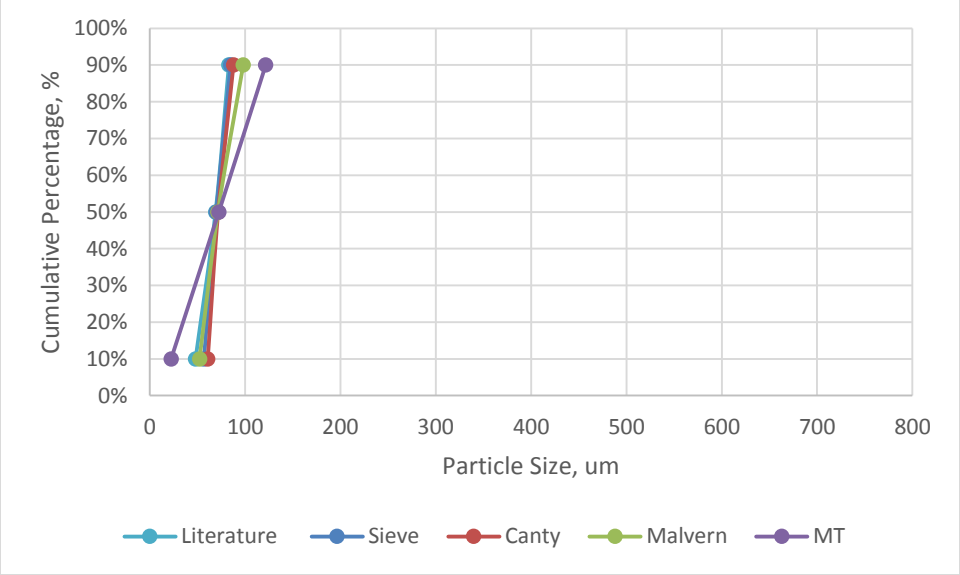

Figure 4- 1 Comparison between the literature data and measurements from sieve analysis, Canty, Malvern and MT for glass microsphere in terms of D10, D50 and D90

The difference between the literature data and the sieve analysis results were calculated and presented in Figure 4-2 in percentage. The most significant difference is found in the comparison of the D10s, i.e. 18.3%. This could have happened due to the settling of smaller particles in the container during transportation or due to the agglomeration of small particles. In the case of D50 and D90, the sieve analysis results are closer to the literature data, which indicates a good quality control on the size of the glass microspheres with less than 2.5% difference with respect to the literature data.

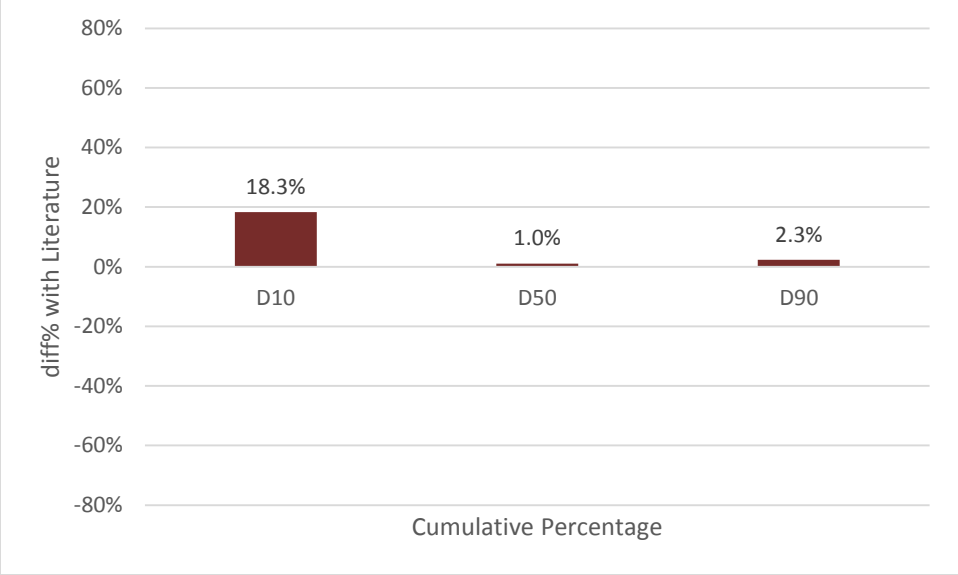

Figure 4- 2 Percentage difference between literature data and measurements from sieve analysis for glass microspheres in terms of D10, D50 and D90

The percentage difference between the sieve analysis results and other measurements is presented in Figure 4-3. In Figure 4-3, it is clear that Canty shows the least difference, while Malvern comes in second.

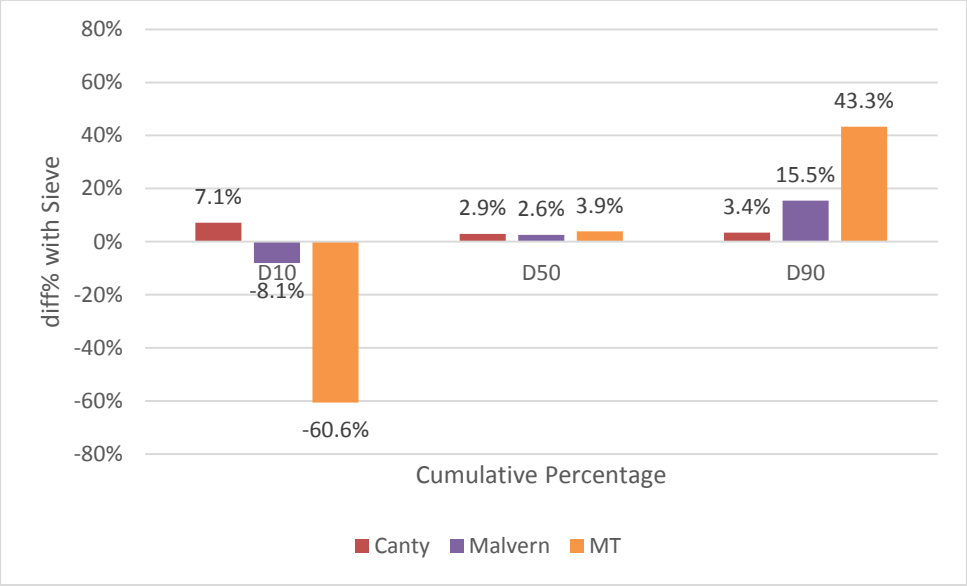

Figure 4- 3 Percentage difference between sieve analysis results and measurements from Canty, Malvern and MT for glass microspheres in terms of D10, D50 and D90

As discussed in the previous chapter, particle size of the glass microspheres should not decrease under the impact of shearing. The measurements of the glass microspheres with increasing shearing time can be used to check the reproducibility of the equipment. These results are shown in Appendix A. The PSD measurements of the five samples with different shearing times obtained using Malvern overlap with each other (Figure A-2). There is a slight discrepancy in the five measurements obtained from MT, but the results are within the acceptable range (Figure A-3). In the case of Canty (Figure A-1), only the PSD measurement obtained for the sample sheared for 30 minutes matches the literature data and the sieve analysis results. All other measurements from Canty shows that larger particles were present in the samples and accounted for 8% in volume, and up to 30% in the extreme case (5-minutes Sample). These large particles turned out to be gas bubbles, which was verified by relating the abnormal particle size in Excel sheets to the particles in the recorded video (Figure 4-4). These gas bubbles might be introduced to the fluid during

the mixing in the mixing tank. Specific particle filter setting can be applied in CantyVisionClient^{TM} software to exclude the gas bubbles. By examining the PSD measurements of the glass microspheres, it is obvious that Malvern and MT tend to have a better reproducibility, while operational errors (introduction of gas bubbles) have a more significant impact on Canty's measurement. This should be taken into consideration when analyzing the results of the size degradation experiments.

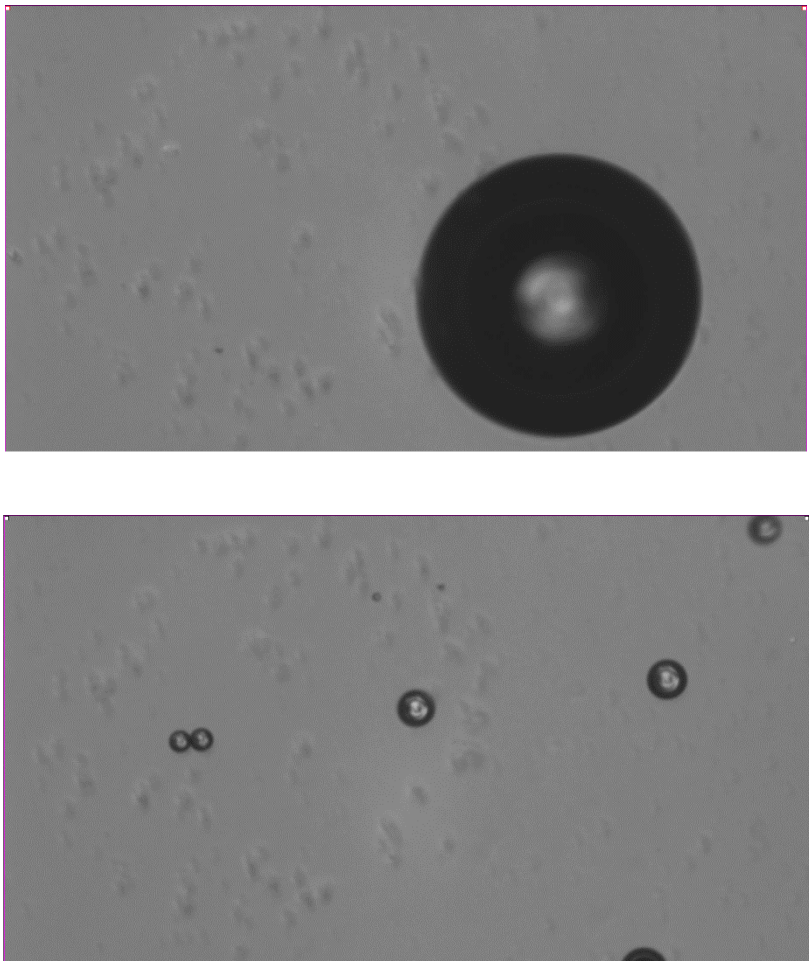

Figure 4- 4 a) Large gas bubble in the fluid analyzed by Canty equipment ; b)Glass microspheres in the fluid have a ring shape appearance;

4.1.2 Calcium Carbonate

There is only one data point (D50) provided as literature data for both calcium carbonate fine (D50 = 150 μm) and calcium carbonate regular (D50 = 250 μm). The comparison between literature data and sieve analysis results for calcium carbonate fine indicates the size of the product is not controlled properly (Table 4-2), while calcium carbonate regular has a better quality control (Table 4-3).

Table 4- 2 Comparison between literature data (D. Clapper, personal communication, September 5th, 2014) and measurements from sieve analysis, Canty, Malvern and MT for calcium carbonate fine in terms of D10, D50 and D90

	D10, μm	D50, μm	D90, μm
Literature Data		150	
Sieve Analysis	25	58	165
Canty	13	25	130
Malvern	4	17	77
MT	19	59	467

Figure 4-5 and Figure 4-6 show that the measurements of calcium carbonate fine from MT agree well with the sieve analysis results on D10 and D50. D90 obtained using MT (467 μm) is significantly higher than the vale obtained from sieve analysis (165 μm). Measurements from Canty and Malvern are lower than the sieve analysis results. The consistency between Canty and Malvern might indicate that small clumps of calcium carbonate might be present at the end of sieving. The vibration applied by sieve shaker is not enough to separate individual calcium carbonate particles, especially for smaller particles (25-165 μm), while the mixing and the flow regime provided by Canty and

Malvern help to separate particles effectively. The explanation described above is only true if the sieving is proven to be ineffective in measuring small particles. Overall, it is hard to tell which equipment performs the best for calcium carbonate fine measurements.

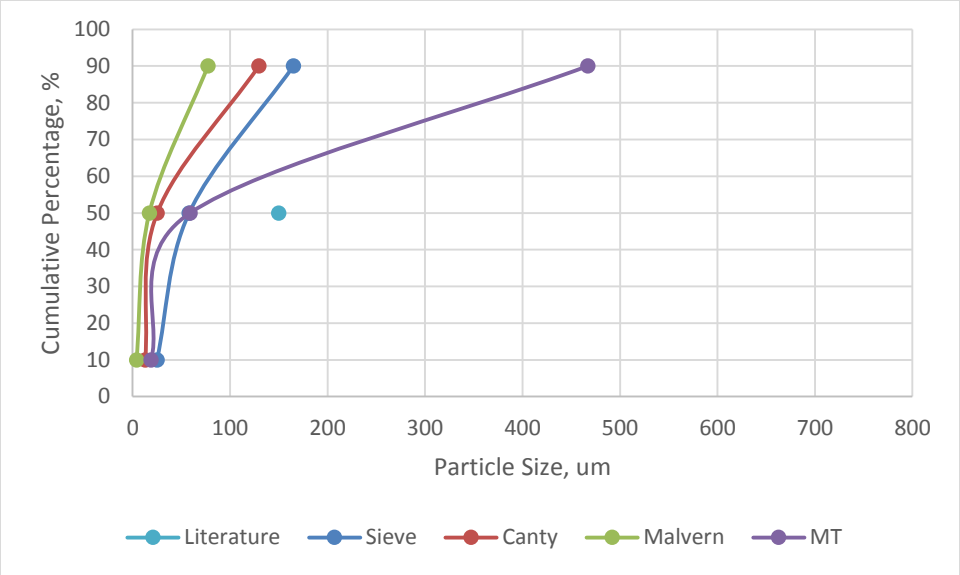

Figure 4- 5 Comparison between literature data and measurements from sieve analysis, Canty, Malvern and MT for calcium carbonate fine in terms of D10, D50 and D90

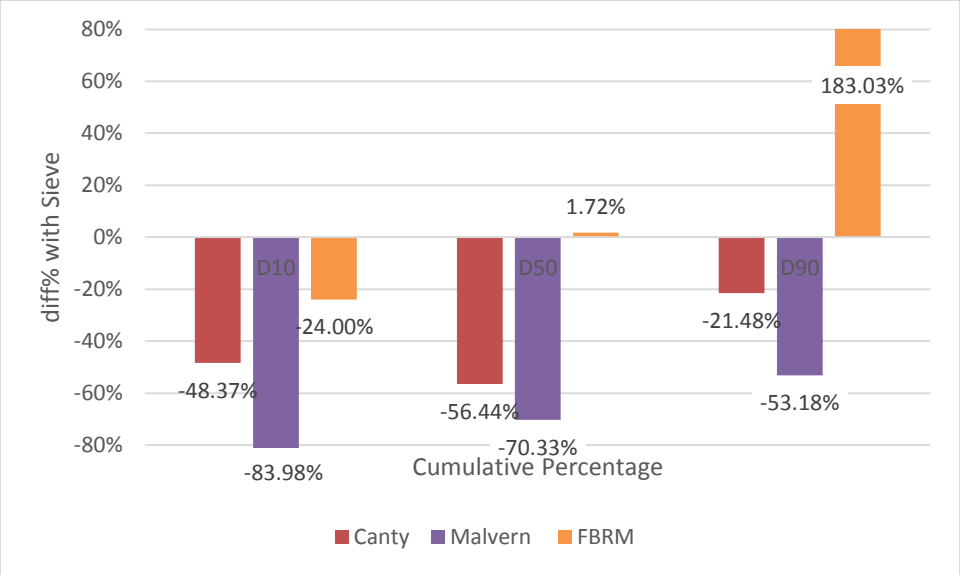

Figure 4- 6 Percentage difference between sieve analysis results and measurements from Canty, Malvern and MT for calcium carbonate fine in terms of D10, D50 and D90

For calcium carbonate regular, measurements (Table 4-3) from the three PSAs follow a similar trend, with a higher D90, lower D10 and similar D50 compared with the results obtained using sieve analysis (Figure 4-7). Figure 4-8 shows that Canty has the least deviation from the sieve analysis results, while MT and Malvern have similar deviations.

Table 4- 3 Comparison between literature data (D. Clapper, personal communication, September 5th, 2014) and measurements from sieve analysis, Canty, Malvern and MT for calcium carbonate regular in terms of D10, D50 and D90

	D10, µm	D50, µm	D90, µm
Literature Data		250	
Sieve Analysis	110	230	338
Canty	60	244	446
Malvern	67	277	508
MT	55	219	468

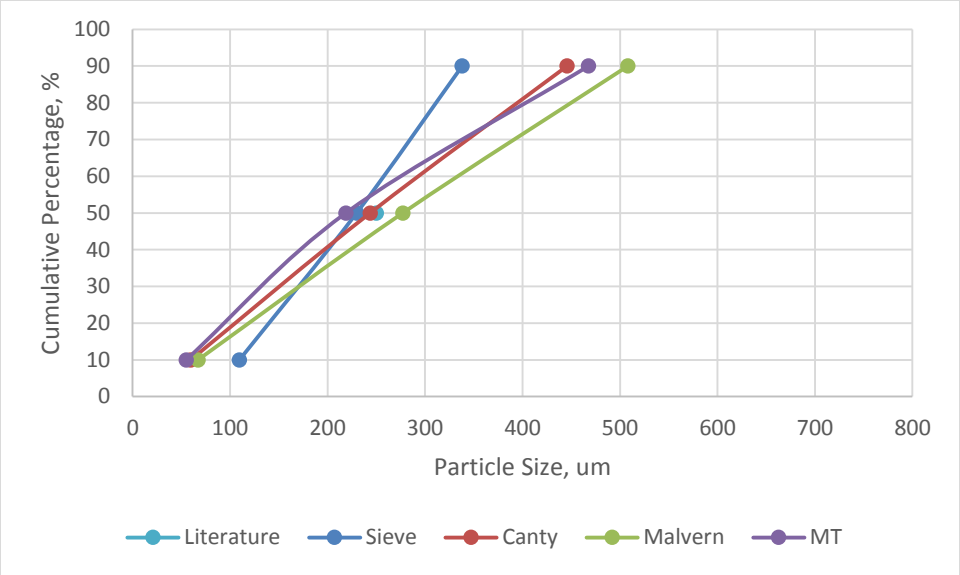

Figure 4- 7 Comparison between literature data and measurements from sieve analysis, Canty, Malvern and MT for calcium carbonate regular in terms of D10, D50 and D90

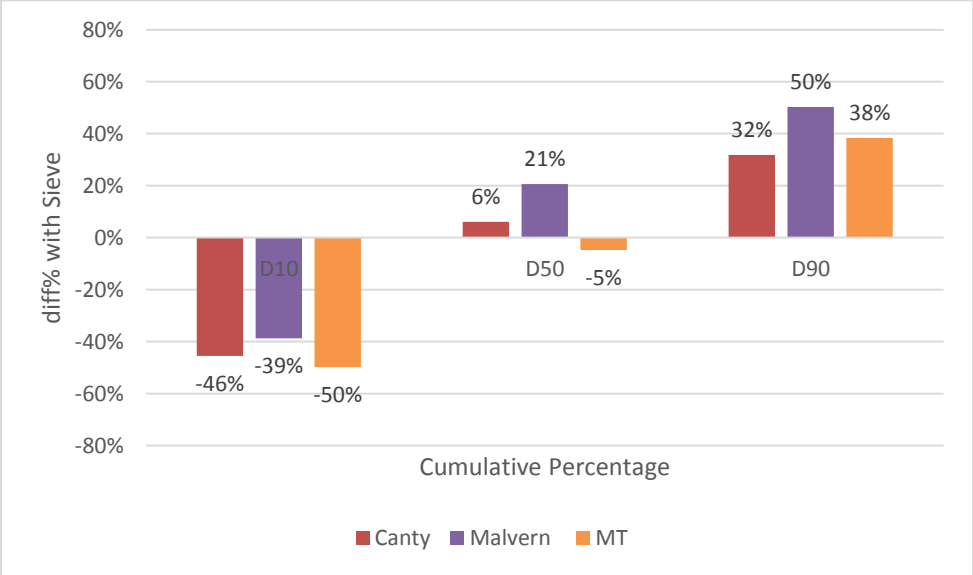

Figure 4- 8 Percentage difference between sieve analysis results and measurements from Canty, Malvern and MT for calcium carbonate regular in terms of D10, D50 and D90

4.1.3 Graphite

Table 4-4, Figure 4-9 and Figure 4-10 shows a good agreement in the value of D50 between sieve analysis results and literature data for graphite fine. The literature data shows a wider particle size distribution compared to the sieve analysis results. The measurements from MT and Canty are consistent with each other, and are lower than the results from sieve analysis. The value of D90 from Malvern matches the value from sieving, with only a 4% difference. However, the values of D50 and D10 from Malvern are significantly lower than those obtained from sieve analysis. Figure 4-11 shows that among the three PSAs, the measurements from Canty have the least difference compared to the values from sieve analysis.

Table 4- 4 Comparison between literature data (D. Clapper, personal communication, September 5th, 2014) and measurements from sieve analysis, Canty, Malvern and MT for graphite fine in terms of D10, D50 and D90

	D10, μm	D50, μm	D90, μm
Literature Data	27	112	287
Sieve Analysis	42	101	223
Canty	38	92	181
Malvern	11	66	215
MT	33	83	178

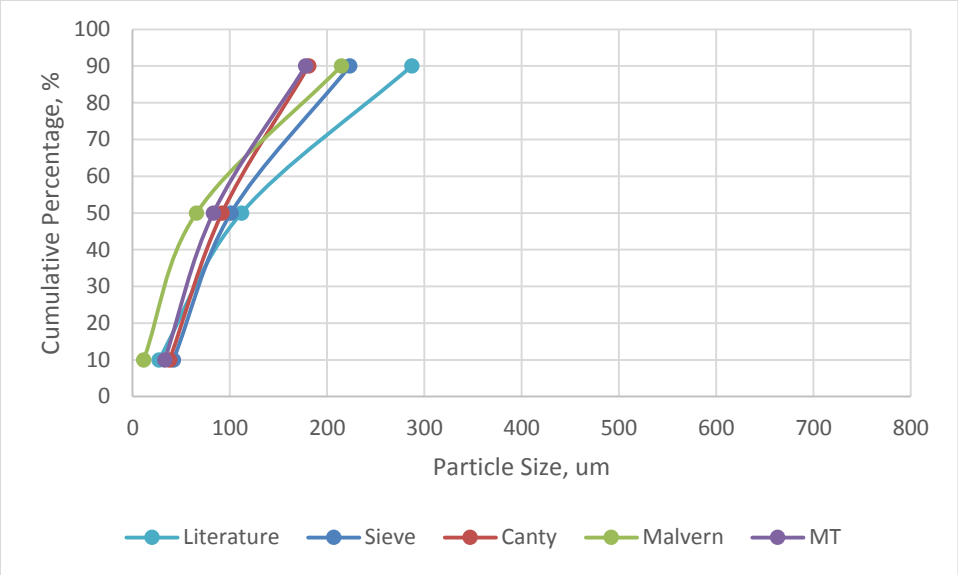

Figure 4- 9 Comparison between literature data and measurements from sieve analysis, Canty, Malvern and MT for graphite fine in terms of D10, D50 and D90

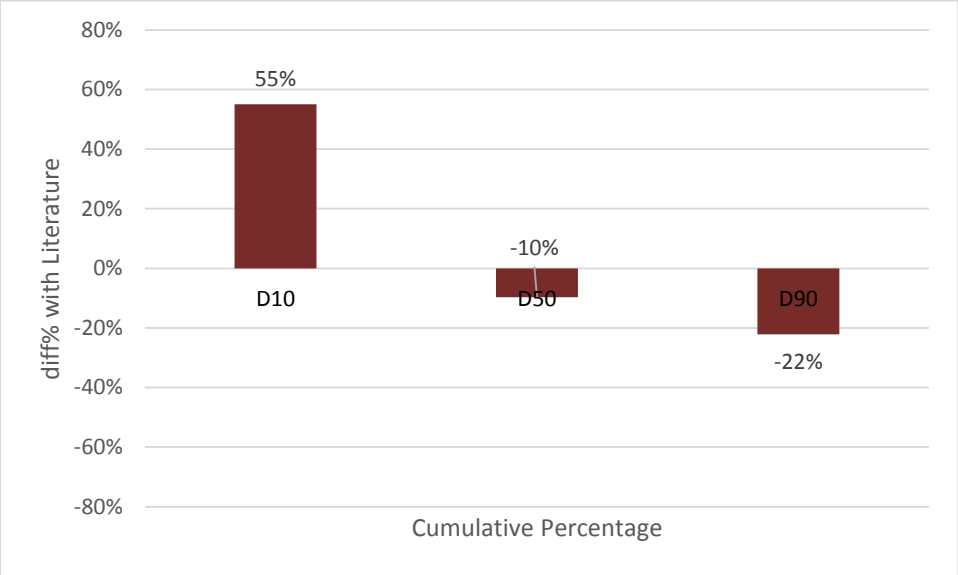

Figure 4- 10 Percentage difference between literature data and measurements from sieve analysis for graphite fine in terms of D10, D50 and D90

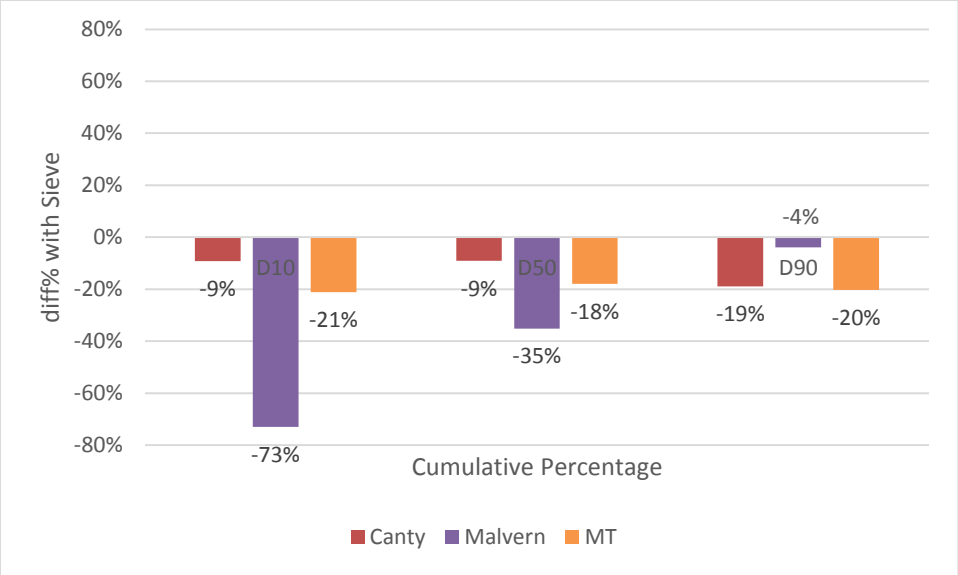

Figure 4- 11 Percentage difference between sieve analysis results and measurements from Canty, Malvern and MT for graphite fine in terms D10, D50 and D90

Table 4-5 and Figure 4-13 present a close match between the sieve analysis results and the literature data for graphite regular. Figures 4-12 and 14 show that the results from Canty have the best match to the sieve analysis results among the three PSAs. It is clear in Figure 4-12 that the measurements from Malvern are higher than the sieve analysis results, while those from MT are lower.

Table 4- 5 Comparison between literature data (D. Clapper, personal communication, September 5th, 2014) and measurements from sieve analysis, Canty, Malvern and MT for graphite regular in terms of D10, D50 and D90

	D10, µm	D50, µm	D90, µm
Literature Data	211	370	634
Sieve Analysis	226	361	628
Canty	230	358	546
Malvern	271	474	781
MT	48	177	501

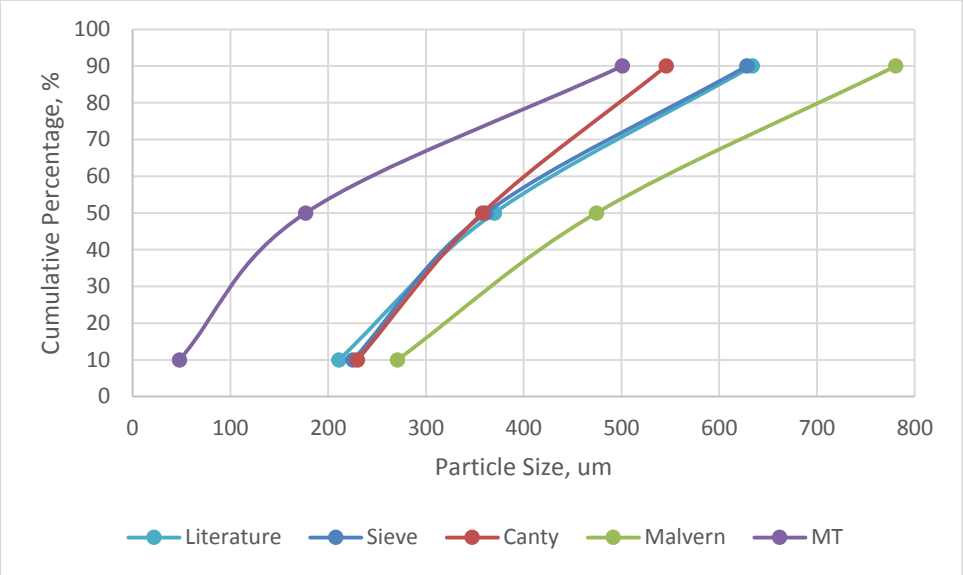

Figure 4- 12 Comparison between literature data and measurements from sieve analysis, Canty, Malvern and MT for graphite regular in terms of D10, D50 and D90

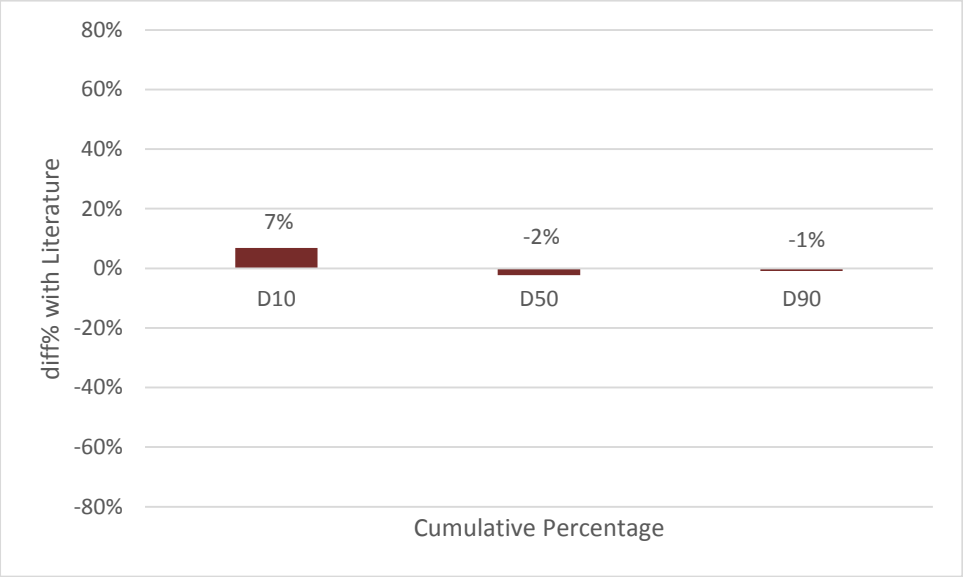

Figure 4- 13 Percentage difference between literature data and measurements from sieve analysis for graphite regular in terms of D10, D50 and D90

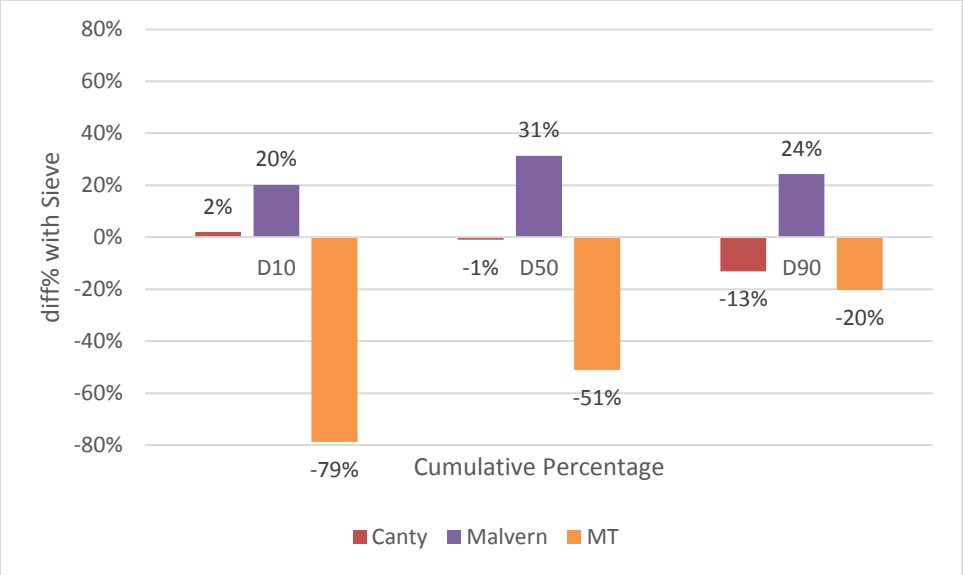

Figure 4- 14 Percentage difference between sieve analysis results and measurements from Canty, Malvern and MT for graphite regular in terms of D10, D50 and D90

The deviation of Malvern's measurements from the sieve analysis in both graphite regular and graphite fine may result from the highly irregular shape of graphite, which is against the assumption of spherical particles.

4.2 Size Degradation Experiments Results

The size degradation experiment was conducted in accordance with the procedure described in section 3.2.2. The results are presented in the following sections, categorized by material type. The analysis is primarily based on the percentage change in the value of D50 with respect to the D50 at the start time of shearing at 0 minute. According to the evaluation in previous section, the measurements from Canty are primarily used in the following analysis. The measurements from Malvern will serve as a supplement to confirm the conclusions. The measurements from MT for calcium carbonate and graphite show undifferentiated size degradation due to shearing, which might be because of its extreme

sensitiveness to the change in particle size. The glass microspheres are used as reference material due to their high hardness and spherical shape. It is in fact shown in section 4.2.1 that the glass microspheres did not experience any shear degradation during the tests.

Graphite regular and calcium carbonate regular experienced the shear degradation to a similar extent, while graphite fine and calcium carbonate did not decrease appreciably in size under the impact of shearing. The results and detailed analysis are presented in section 4.2.2 and 4.2.3. As to the original size of calcium carbonate and graphite increases, the ease by which the material breaks down is consistent with Scott's findings (Scott et al. 2012).

4.2.1 Glass Microsphere

Figure 4-15 shows the change in value of D50 with increasing shearing time. Though there was some fluctuation in the data obtained from MT, the difference between 0 minute and 20 minutes measurements was only 10%, which is only an 8 μm difference in reality. All the measurements show that glass microspheres did not experience shear degradation as the shearing time was increased. This information can also confirmed based on the data presented in Table 4-6.

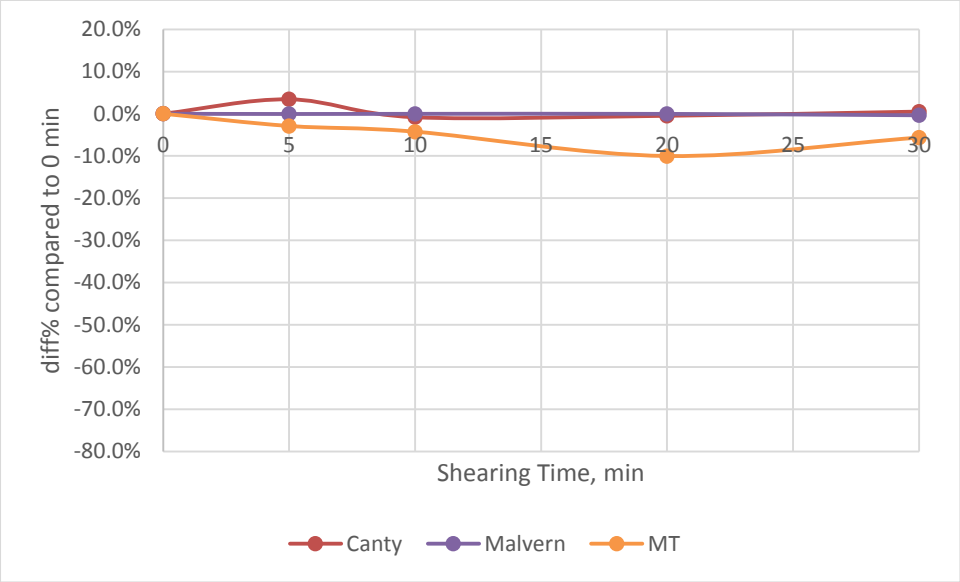

Figure 4- 15 Changes in the value of D50 of glass microspheres with increasing shearing time in terms of D50 according to measurements of Canty, Malvern and Mettler Toledo PSAs

Table 4- 6 Changes in the value of D50 of glass microspheres with increasing shearing time in terms of D50 according to measurements of Canty, Malvern and Mettler Toledo PSAs

	Canty		Malvern		MT	
Shearing Time, min	D50, µm	Diff% compared to 0 min	D50, µm	Diff% compared to 0 min	D50, µm	Diff% compared to 0 min
0	72	0.0%	72	0.0%	75	0.0%
5	74	3.4%	71	-0.1%	73	-2.9%
10	71	-0.8%	72	0.0%	72	-4.3%
20	71	-0.5%	71	0.0%	67	-10.0%
30	72	0.5%	71	-0.4%	71	-5.6%

4.2.2 Calcium Carbonate

For calcium carbonate fine, there is a difference between value of D50 for the samples sheared for 0 minute and for 5 minutes using MT, 38% (Figure 4- 16 and Table 4-7). This difference goes up as the shearing time goes up. This is most likely due to insufficient initial dispersion of the material, which clumps together at first and then separates, creating the illusion of large initial shear degradation. Shearing for 0 minute was achieved by stirring the sample using a spatula, which might not be enough shear to disperse the smaller particles contained in the sample (calcium carbonate fine has particle size ranging from 25 to 165 μm). For the lab setup, MT operated at 400 rpm and an undiluted sample was used during measurement. Low mixing speed along with the use of an undiluted sample did not help with the dispersion. On the other hand, in the Malvern, the sample was pumped at 2000 rpm and the representative sample was diluted with deionized water. Dilution of a sample is generally not desirable, but it helps with dispersion of particles in the fluid. It is a similar case with Canty: dilution helps with dispersion. Although measurements from Canty fluctuated around 25 μm (0-minute measurement), the variations are acceptable. Measurements from Malvern for 5-, 10-, 20- and 30- minutes are almost the same, indicating that no further degradation occurred with additional shearing time beyond 5 minutes. In general, it is fair to conclude that calcium carbonate fine does not experience shear degradation to a noticeable extent.

In the case of calcium carbonate regular, all PSAs showed good agreement in the results (Figure 4-17 and Table 4-8), which indicate that calcium carbonate regular experienced shear degradation and the average reduction in size (D50) after 30-minutes shearing was approximately 35% according to Canty and MT equipment. And about 30% according to Malvern

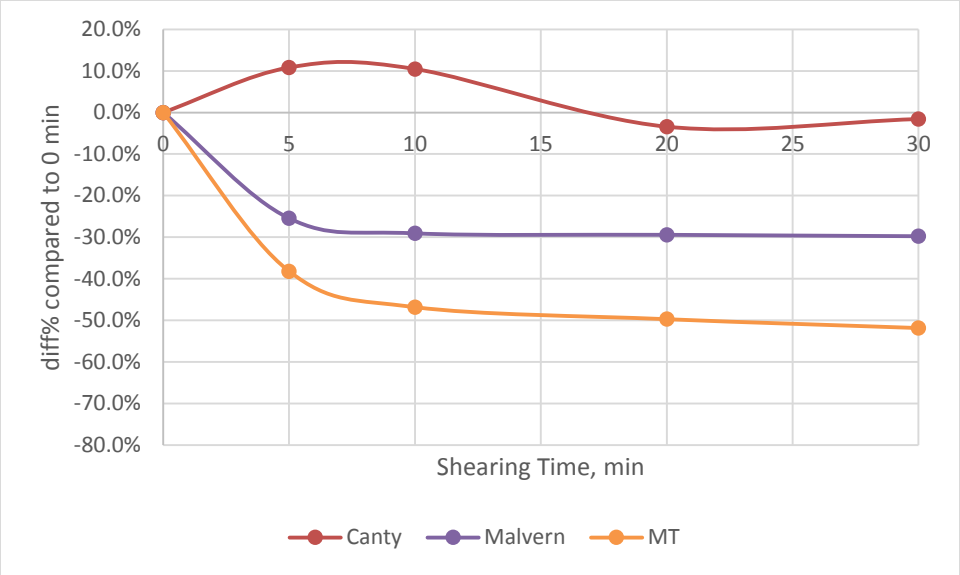

Figure 4- 16 Changes in the value of D50 of calcium carbonate fine with increasing shearing time in terms of D50 according to measurements of Canty, Malvern and Mettler Toledo PSAs

Table 4- 7 Changes in the value of D50 of calcium carbonate fine with increasing shearing time in terms of D50 according to measurements of Canty, Malvern and Mettler Toledo PSAs

	Canty		Malvern		MT	
Shearing Time, min	D50, µm	%Diff compared to 0 min	D50, µm	%Diff compared to 0 min	D50, µm	%Diff compared to 0 min
0	25	0.0%	17	0.0%	59	0.0%
5	28	10.8%	13	-25.4%	36	-38.2%
10	28	10.5%	12	-29.1%	31	-46.8%
20	24	-3.4%	12	-29.4%	29	-49.7%
30	25	-1.6%	12	-29.8%	28	-51.8%

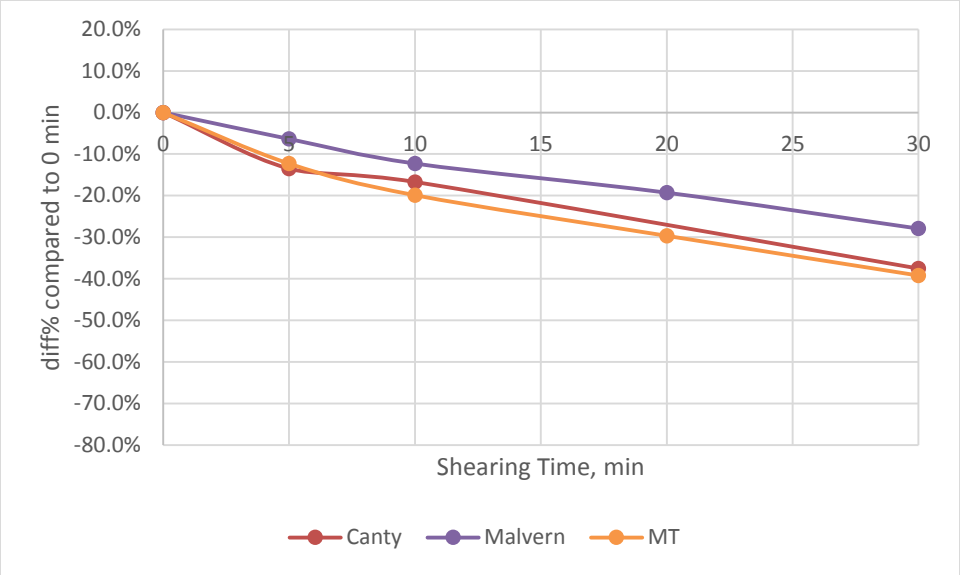

Figure 4- 17 Changes in the value of D50 of calcium carbonate regular with increasing shearing time in terms of D50 according to measurements of Canty, Malvern and Mettler Toledo particle size analyzers

Table 4- 8 Changes in the value of D50 of calcium carbonate regular change with increasing shearing time in terms of D50 according to measurements of Canty, Malvern and Mettler Toledo PSAs

	Canty		Malvern		MT	
Shearing Time, min	D50, µm	%Diff compared to 0 min	D50, µm	%Diff compared to 0 min	D50, µm	%Diff compared to 0 min
0	244	0.0%	277	0.0%	216	0.0%
5	211	-13.5%	260	-6.4%	190	-12.3%
10	203	-16.7%	243	-12.3%	173	-19.9%
20	N/A	N/A	224	-19.3%	152	-29.7%
30	152	-37.5%	200	-27.9%	131	-39.2%

4.2.3 Graphite

Similar to the trend observed in calcium carbonate fine (in section 4.2.2), it was that graphite fine particles were not completely dispersed in the 0 minutes sample measured using MT. This resulted in a significant size reduction from the 0-minute to 5-minutes samples (Figure 4-18 and Table 4-9). Upon further shearing, the size of graphite fine measured by MT did not change significantly from the 5-minutes sample. Besides an abnormal measurement of the 5-minutes sample from Canty, most measurements from Canty and Malvern shows that graphite fine did not experience shear degradation. The abnormal measurement from Canty might be due to operational errors or large particles that were potentially trapped in the neck section of the equipment connecting the reservoir tank and the tubing, which were therefore not analyzed.

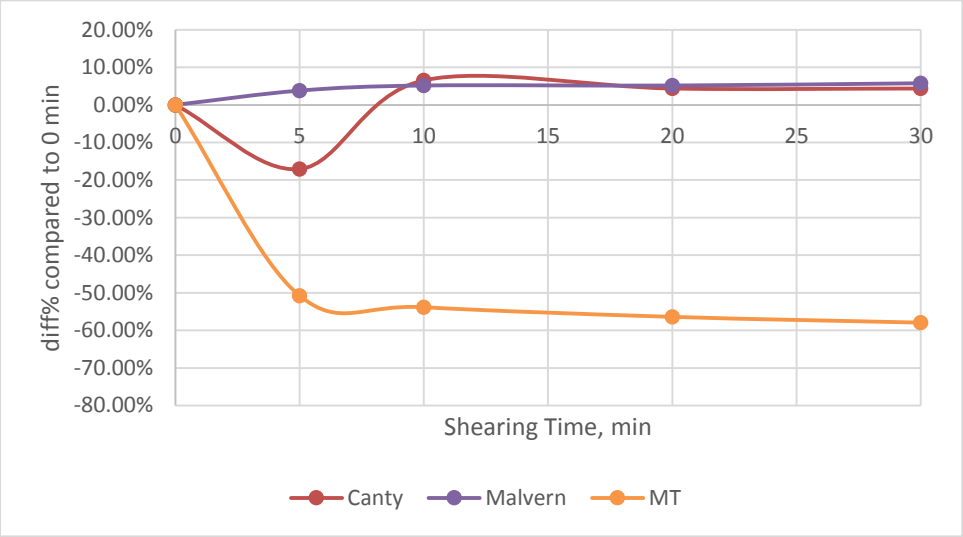

Figure 4- 18 Changes in the value of D50 of graphite fine with increasing shearing time in terms of D50 according to measurements of Canty, Malvern and Mettler Toledo PSAs

Table 4- 9 Changes in the value of D50 of graphite fine with increasing shearing time in terms of D50 according to measurements of Canty, Malvern and Mettler Toledo PSAs

	Canty		Malvern		MT	
Shearing Time, min	D50, μm	%Diff compared to 0 min	D50, μm	%Diff compared to 0 min	D50, μm	%Diff compared to 0 min
0	92	0.0%	66	0.0%	98	0.0%
5	76	-17.1%	69	3.8%	48	-50.8%
10	98	6.5%	69	5.2%	45	-53.8%
20	96	4.3%	69	5.2%	43	-56.4%
30	96	4.3%	70	5.8%	41	-57.9%

For graphite regular, the D50 values obtained from MT shows a much larger reduction in size compared to that from Malvern and Canty. This might be because the particle size measured using MT is the chord length of the particles. Thus, MT's equipment is more sensitive to the change in the particle size, but might exaggerate the change as the particle shape become more irregular. Although there are some fluctuations in Canty and Malvern's measurements, which might due to the sampling and the operational errors, from the overall trend it is obvious that graphite regular experienced shear degradation of an order of magnitude that is slightly less but still comparable to the degradation of calcium carbonate regular, i.e. 20 – 35%.

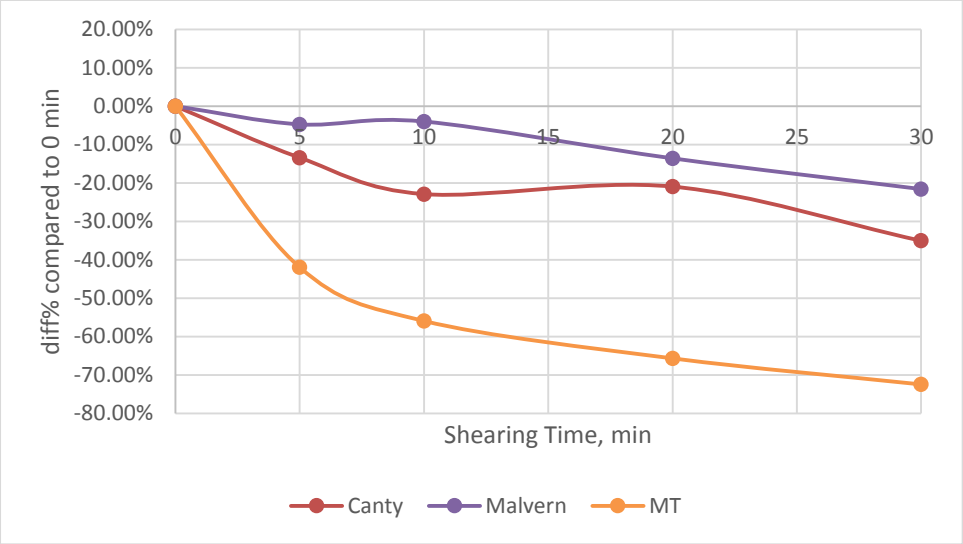

Figure 4- 19 Changes in the value of D50 of graphite regular with increasing shearing time in terms of D50 according to measurements of Canty, Malvern and Mettler Toledo PSAs

Table 4- 10 Changes in the value of D50 of graphite regular with increasing shearing time in terms of D50 according to measurements of Canty, Malvern and Mettler Toledo PSAs

	Canty		Malvern		MT	
Shearing Time, min	D50, µm	%Diff compared to 0 min	D50, µm	%Diff compared to 0 min	D50, µm	%Diff compared to 0 min
0	358	0.0%	475	0.0%	236	0.0%
5	310	-13.4%	452	-4.7%	137	-41.9%
10	276	-22.9%	456	-4.0%	104	-55.9%
20	283	-20.9%	410	-13.6%	81	-65.7%
30	233	-35.1%	372	-21.6%	65	-72.5%

4.2.4 Rheology Measurements

This section presents the rheology measurements in the size degradation experiment for glass microspheres, calcium carbonate regular and graphite regular. Tables 4-11, 4-12 and 4-13 show that there is no significant change in rheological properties as the shearing time increases. It might be due to the small concentration of the lost circulation materials in the fluid.

Table 4- 11 Rheological properties of the glass microsphere samples with different shearing time

	0 min	5 mins	10 mins	20 mins	30 mins
PV, cp	3.8	3.8	4.3	4.1	4.2
YP, lb/100 ft^2	14.1	14.8	13.8	14	13.7
10 sec gel, lb/100 ft^2	5.3	6.1	5.6	5.7	5.8
Dial Readings @ 120 °F					
600 RPM	21.7	22.4	22.4	22.2	22.1
300 RPM	17.9	18.6	18.1	18.1	17.9
200 RPM	16.1	16.2	16.2	16.2	16.5
100 RPM	13.1	13.8	13.5	13.4	13.7
6 RPM	6.4	6.8	6.7	6.9	6.6
3 RPM	5	5.6	5	5.3	5.6

Table 4- 12 Rheological properties of calcium carbonate regular samples with different shearing time

	0 min	5 mins	10 mins	20 mins	30 mins
PV, cp	3.7	2.9	2.8	4.3	2.5
YP, lb/100 ft^2	13.9	15	14.6	13.1	16.5
10 sec gel, lb/100 ft^2	6.1	6	5.6	5.9	5.7
Dial Readings @ 120 °F					
600 RPM	21.3	20.8	20.2	21.7	21.5
300 RPM	17.6	17.9	17.4	17.4	19
200 RPM	15.6	15.9	15.5	15.6	16.3
100 RPM	13.3	13.4	12.8	13.4	13.8
6 RPM	6.5	6.6	6.1	6.8	6.7
3 RPM	5.4	5.2	5.4	5.5	5.1

Table 4- 13 Rheological properties of graphite regular samples with different shearing time

	0 min	5 mins	10 mins	20 mins	30 mins
PV, cp	4.3	4.5	3.9	4.2	4.2
YP, lb/100 ft^2	13	13.4	13.6	13.1	13.1
10 sec gel, lb/100 ft^2	5.8	6.3	5.8	5.8	6
Dial Readings @ 120 °F					
600 RPM	21.6	22.4	21.4	21.5	21.5
300 RPM	17.3	17.9	17.5	17.3	17.3
200 RPM	15.9	16.4	15.9	15.9	15.9
100 RPM	13.3	13.1	13.3	13.3	12.9
6 RPM	6.2	7	6.4	6.5	6.6
3 RPM	5.4	5.7	5.2	5.4	5.3

Chapter 5: Conclusions and Future Works

5.1 CONCLUSIONS

It is crucial to have a good understanding of the PSD in drilling fluids. An accurate PSD measurement could be obtained through trending laser technology or visual image analysis. Among three commercial PSAs introduced and used in this study, Canty Drilling Mud Particle Size Analyzer generates more accurate quantitative results for the common materials used in drilling fluids. Although sample dilution is required, the video recording and visual verification features provided by Canty distinguish it from the other two PSAs. However, during this study it was found that reproducibility of results is a metter of a concern. Human error has a higher impact on the results obtained from Canty than from the other PSAs. Canty's software has a high flexibility and allows users to apply sophisticated particle filters. However, it also requires experienced users to reach its best performance.

The prominent advantage of Mettler Toledo ParticleTrack G400 is it is the easiest to operate and that sample dilution is not required for testing. The dilution process may comprise drilling fluid properties, especially for oil/synthetic based mud (a follow-up study is currently being conducted to investigate this issue). This equipment by Mettler Toledo has been used on rigs in field practice and could be easily incorporated into any currently existing flow loop by simply incorporating the probe into the tubing (ideally installed in a turbulent flow section) to monitor particle size in real-time. According to a previous field applications, MT was found to be sensitive to small change in particle size (Ronaes, Fossdal, and Stock 2012). In this study, the results obtained from MT are distinctly different from thoese of other PSA methods. This is due to the fact that MT measures chord

length of the particles. The output chord length distribution must be converted to a regular PSD for comparison, during which simplifications and errors are introduced.

The Malvern Mastersizer 2000 is the most reliable equipment with excellent repeatability, easy operation and fast response. The inaccuracy in measurements from Malvern increases as particle shape becomes more irregular, owing to its assumption that all particles are spherical. Malvern requires dilution as well. Malvern and MT cannot distinguish bubbles/droplets from particles. If any bubbles or droplets are present in the fluid, such as invert emulsion oil-based mud, Malvern and MT will treat the bubbles and the droplets as particles, resulting in a false PSD. However, Canty can be used with a particle filter and the PSD can be correlated with the images to distinguish bubbles/droplets from particles.

Based on this study, if Canty's reproducibility can be improved and its operating process simplified, especially during the data analysis stage, it could serve as a good candidate for accurate particle size measurement on the rigsite. The only realistic candidate for rig site deployment and automation right now is the MT equipment, but its method for determining PSD's needs to be improved.

The particle size of common materials used in drilling fluids is within 1-100 μm. The materials contributing to wider PSD with larger particles are LCMs such as calcium carbonate and graphite. Any size reduction in these LCMs has a significant impact on the overall PSD. It has been shown in our study that, 1) 200-650 μm graphite and 100-350 μm calcium carbonate experienced a reduction in particle size when a high shear is applied; 2) As the initial size of LCMs decreases, the size reduction is smaller or even diminishes; 3) As the shearing time increases, the material continues to break down until it is small enough; 4) Graphite is slightly more shear resistant than calcium carbonate.

5.2 FUTURE WORK

As mentioned in Chapter 2, there are several other particle size measurement techniques available but not discussed or employed in this study, such as ultrasonic extinction. Evaluation of other techniques might be of value in determining the optimal particle sizing technique for both laboratory and field applications. This study focused on comparing particle size measurements experimentally. The mathematical understanding of PSD from different techniques might help to further explain - and improve upon - the inconsistency in measurements obtained from different equipment.

Calcium carbonate and graphite are widely used LCM in the industry. But there are other popular LCMs, such as nut hulls. Other bridging materials could be investigated to identify the one with highest shear resistance. To better simulate downhole conditions and to develop a reliable quantitative relationship between size reduction and the shear experienced by a material, it is suggested to develop a flow loop setup with nozzles that can actually simulate the effect of drilling fluid and its components passing through a drill bit, i.e. the place where highest shear is imparted.

Appendix A: Cumulative Particle Size Distribution Graphs

This appendix includes cumulative PSD of glass microspheres, calcium carbonate fine, calcium carbonate regular, graphite fine and graphite regular measured using Canty Drilling Mud Particle Size Analyzer, Malvern Mastersizer 2000 and Mettler Toledo ParticleTrack G400.

A.1 Glass Microsphere

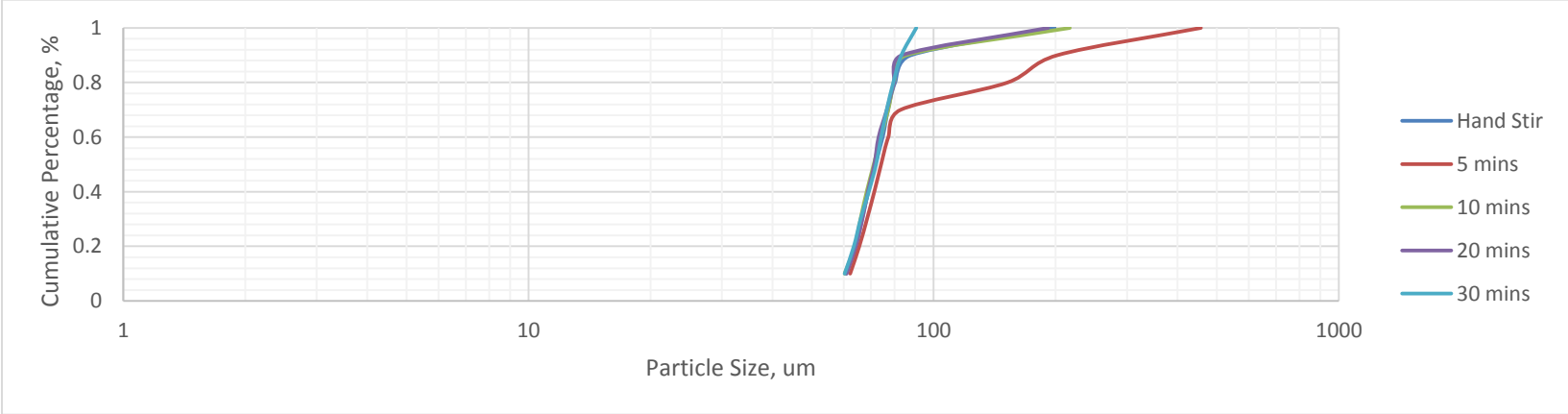

Figure A- 1 Cumulative PSD using Canty with increasing shearing time for glass microspheres

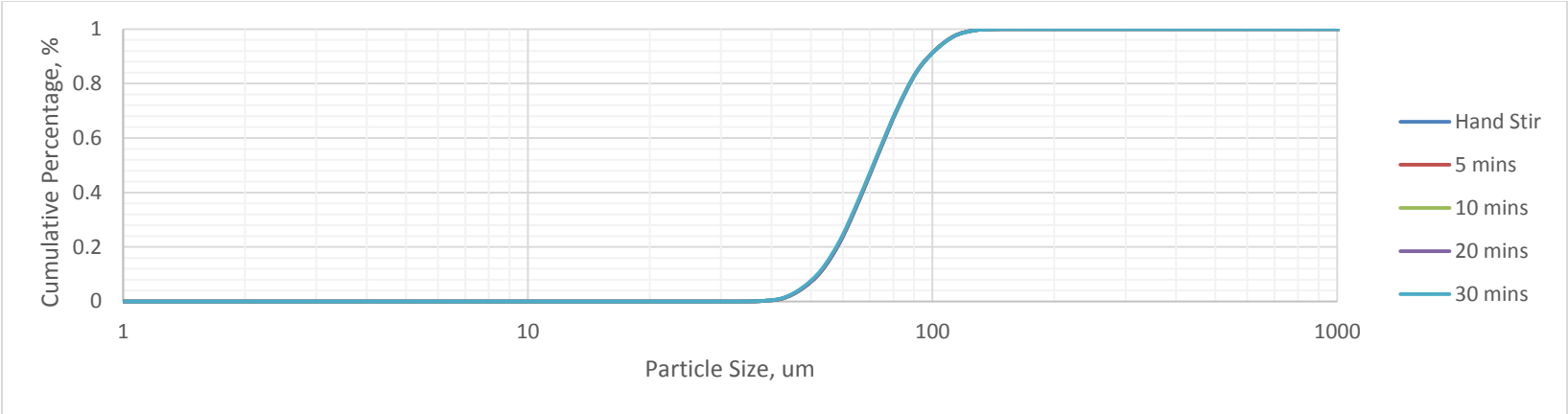

Figure A- 2 Cumulative PSD using Malvern with increasing shearing time for glass microspheres

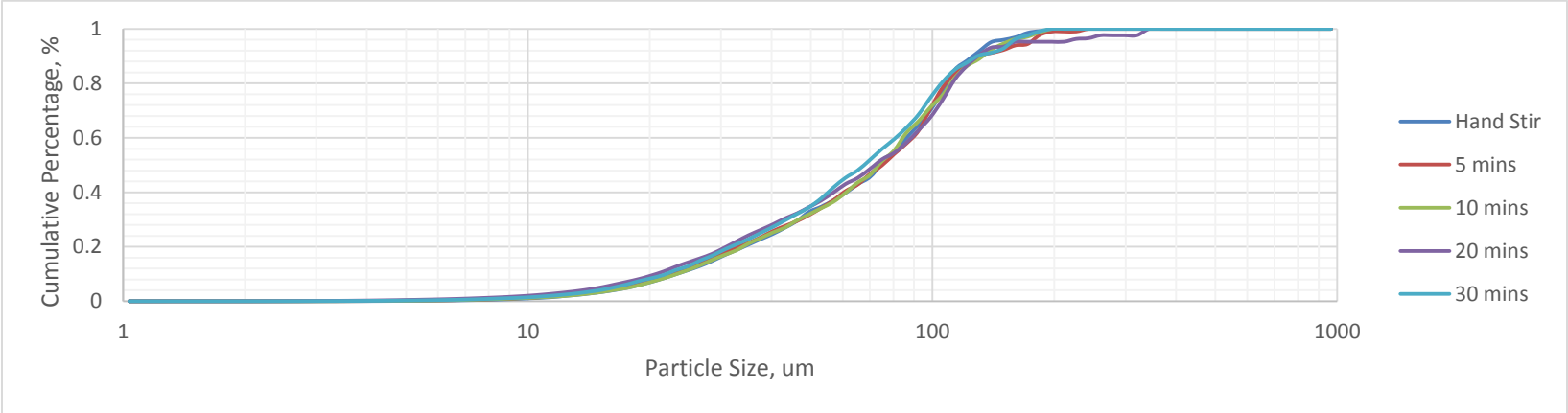

Figure A- 3 Cumulative PSD using MT with increasing shearing time for glass microspheres

A.2 Calcium Carbonate Fine

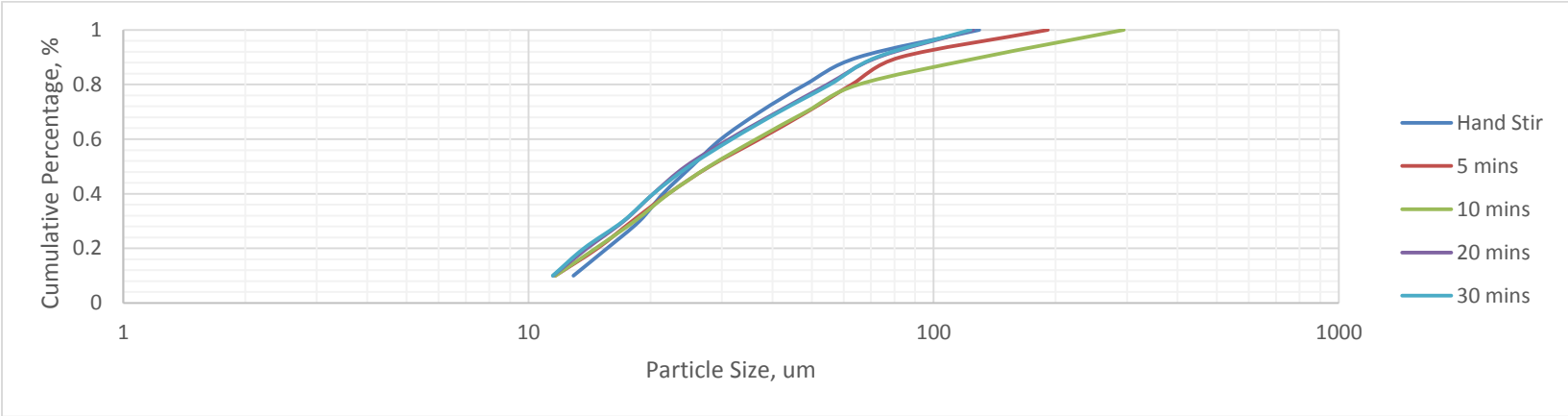

Figure A- 4 Cumulative PSD using Canty with increasing shearing time for calcium carbonate fine

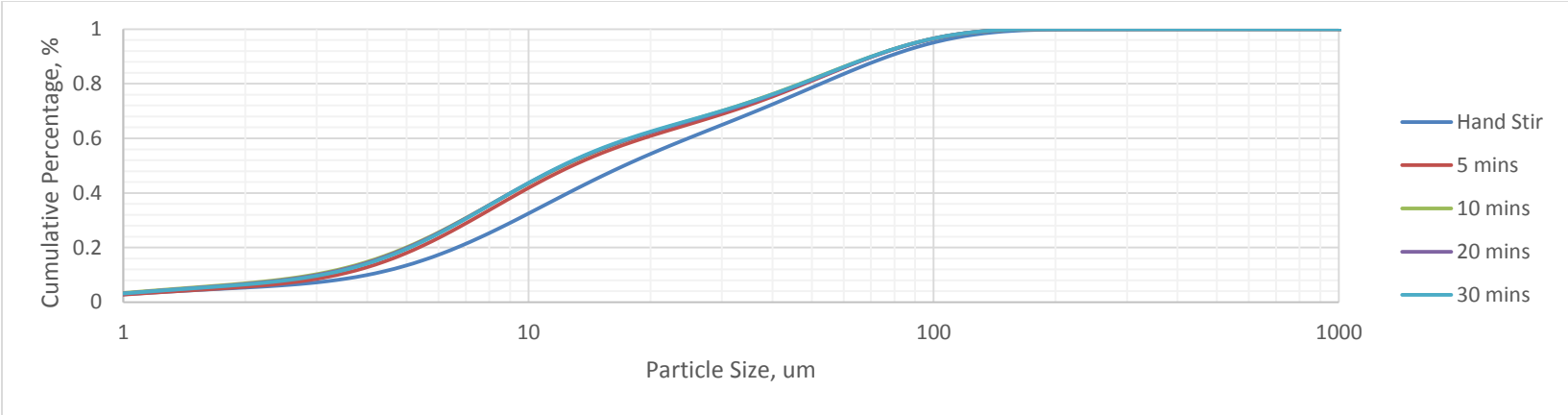

Figure A- 5 Cumulative PSD using Malvern with increasing shearing time for calcium carbonate fine

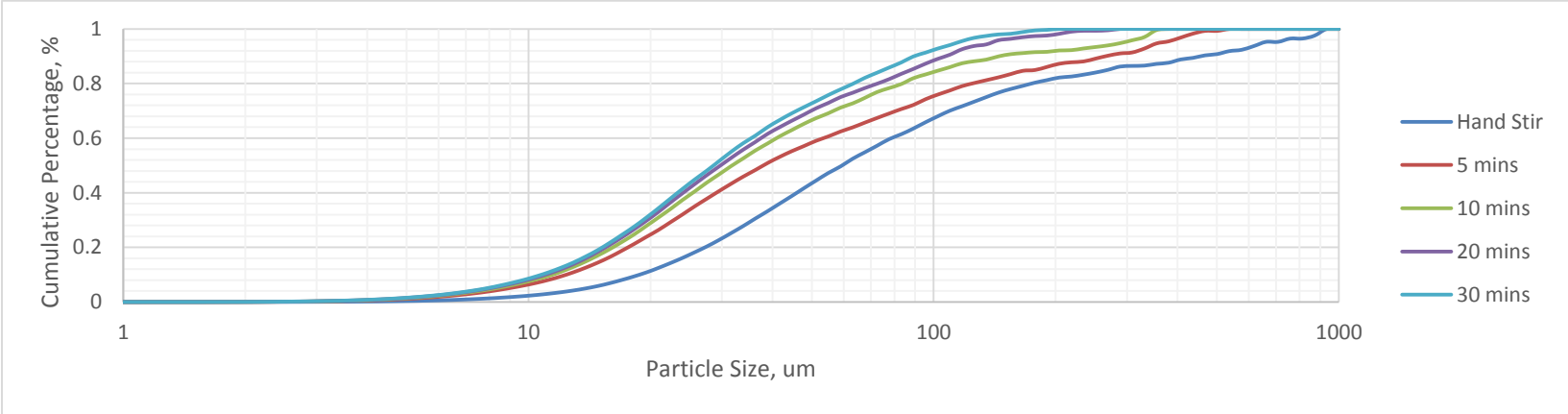

Figure A- 6 Cumulative PSD using MT with increasing shearing time for calcium carbonate fine

A.3 Calcium Carbonate Regular

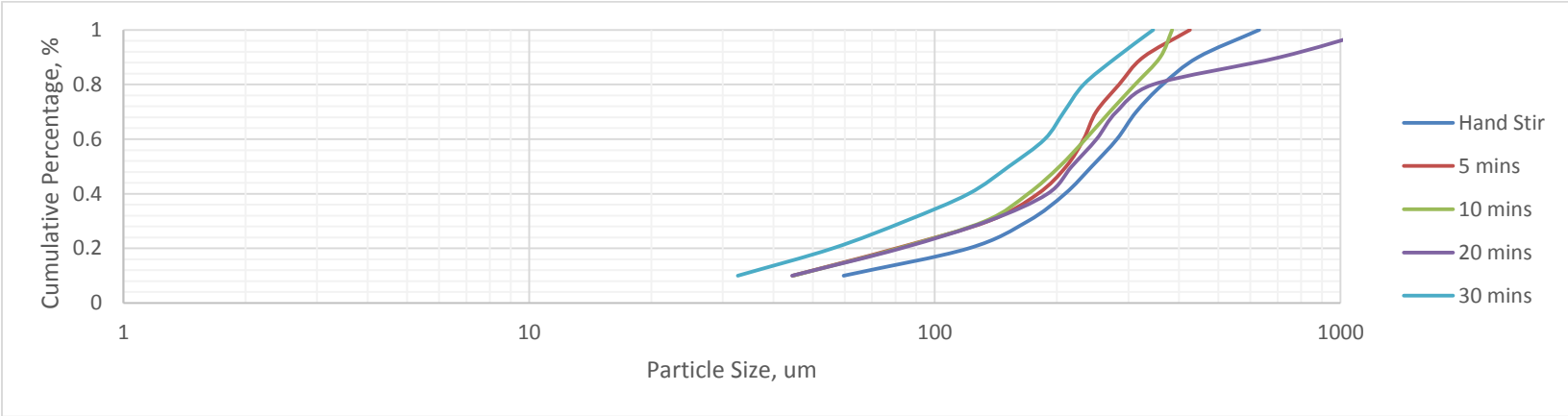

Figure A- 7 Cumulative PSD using Canty with increasing shearing time for calcium carbonate regular

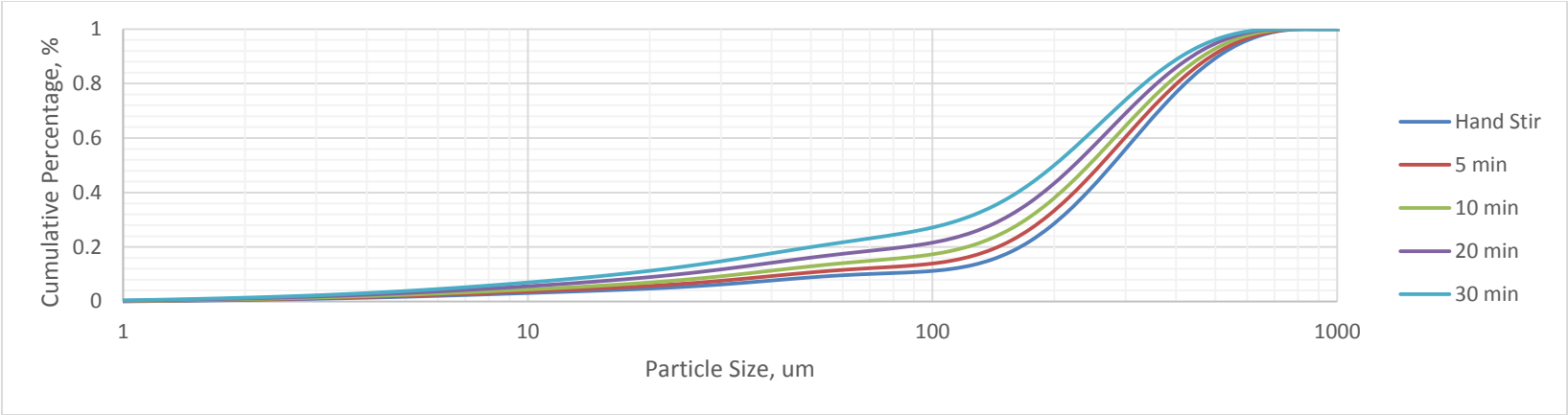

Figure A- 8 Cumulative PSD using MT with increasing shearing time for calcium carbonate regular

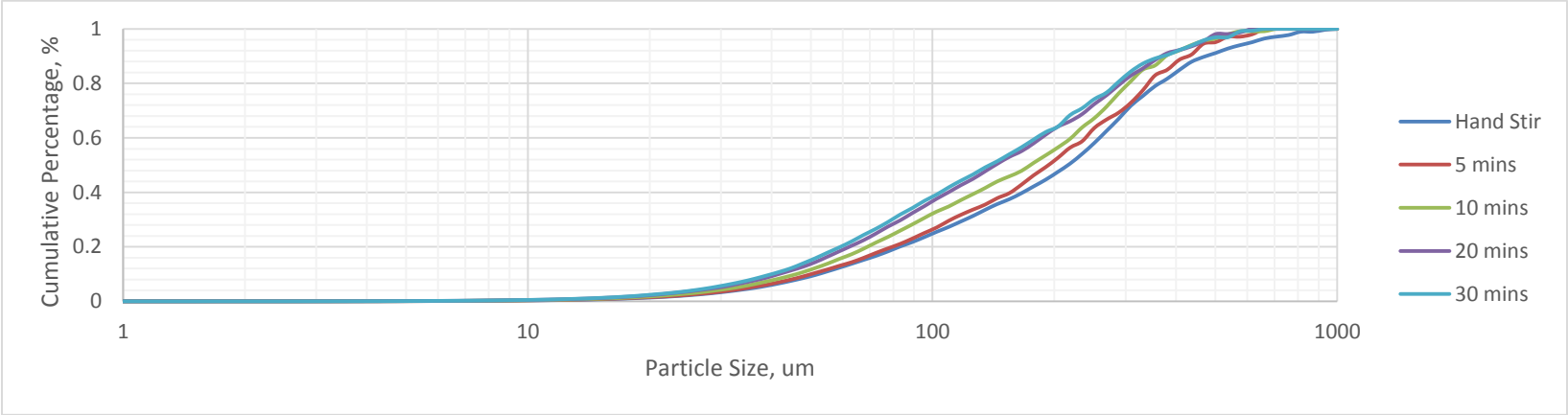

Figure A- 9 Cumulative PSD using MT with increasing shearing time for calcium carbonate regular

A.4 GRAPHITE FINE

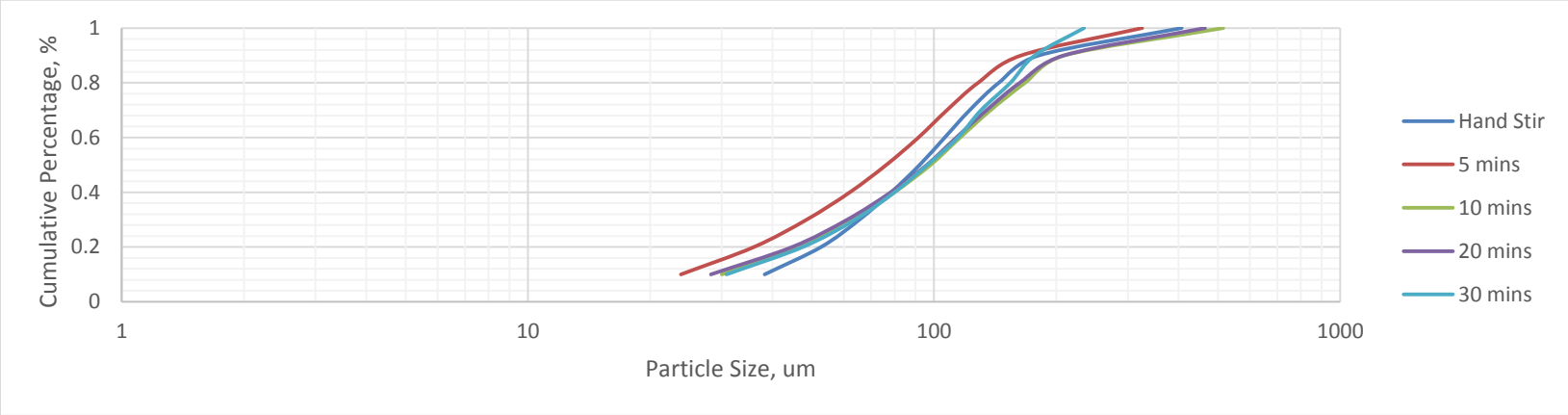

Figure A- 10 Cumulative PSD using Canty with increasing shearing time for graphite fine

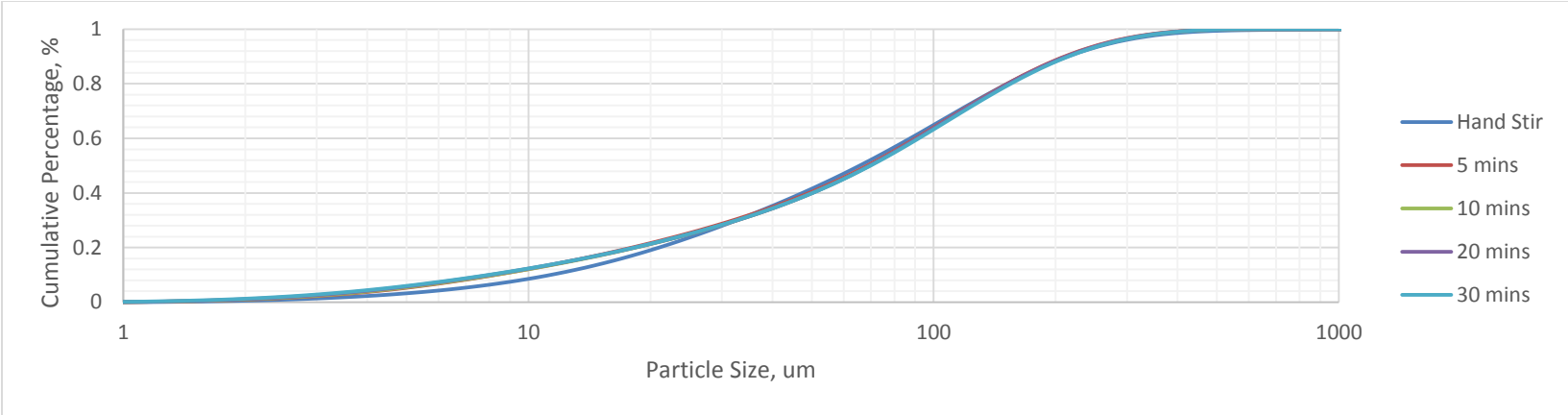

Figure A- 11 Cumulative PSD using Malvern with increasing shearing time for graphite fine

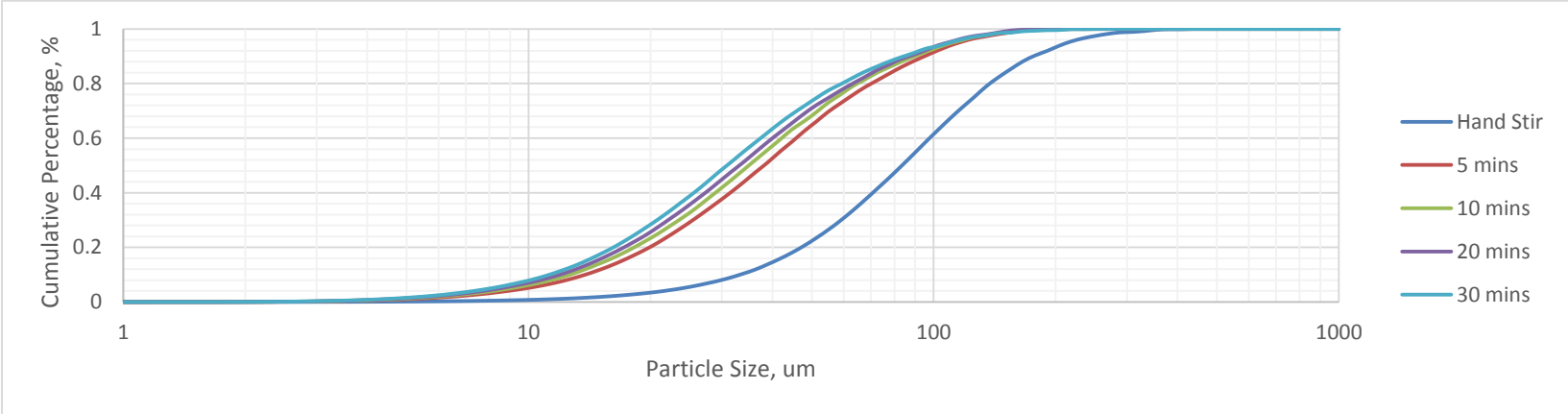

Figure A- 12 Cumulative PSD using MT with increasing shearing time for graphite fine

A.5 GRAPHITE REGULAR

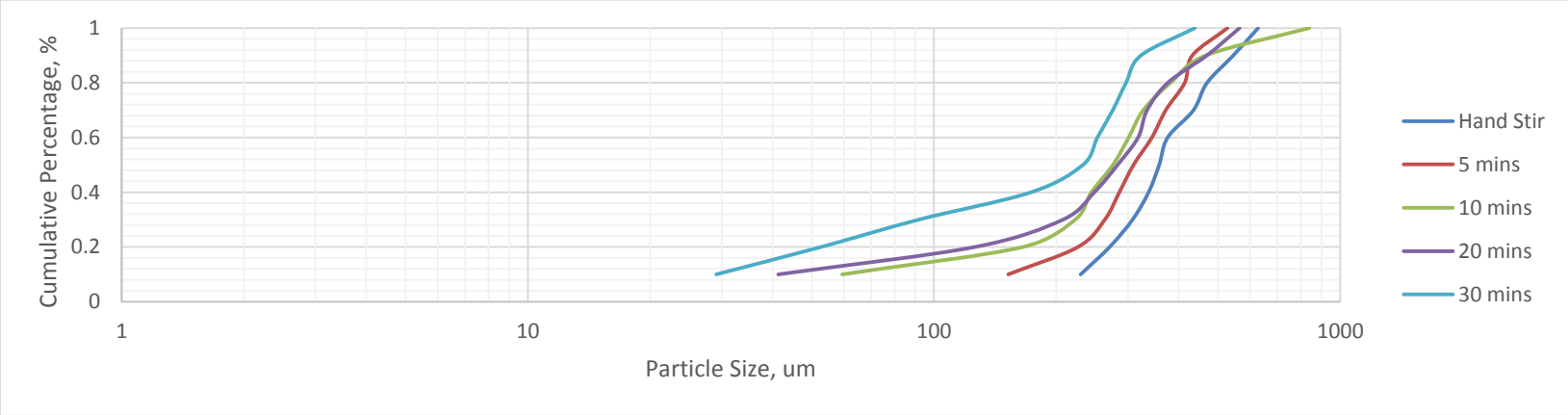

Figure A- 13 Cumulative PSD using Canty with increasing shearing time for graphite regular

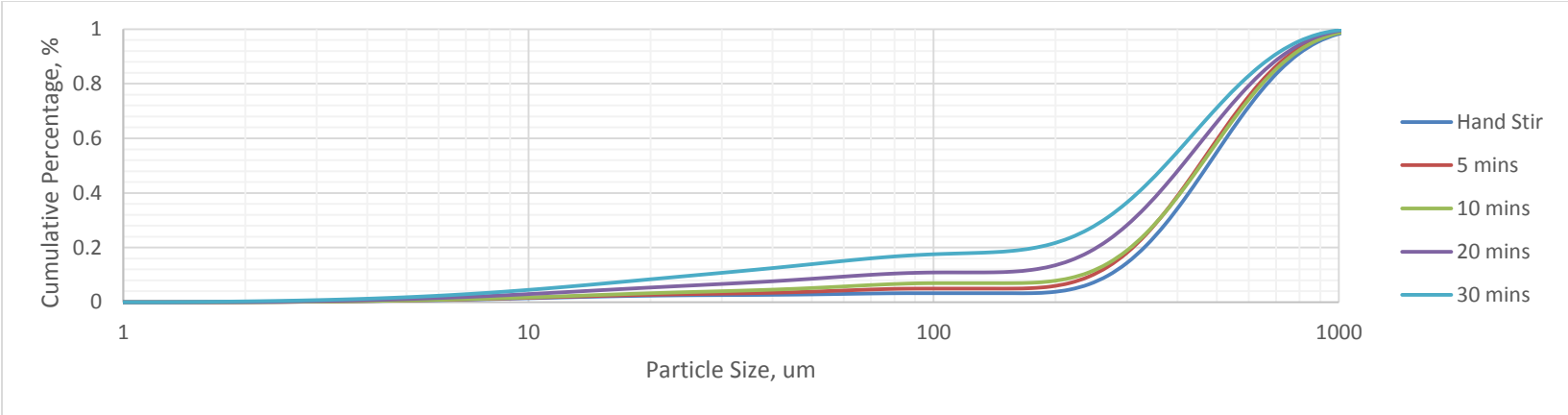

Figure A- 14 Cumulative PSD using Malvern with increasing shearing time for graphite regular

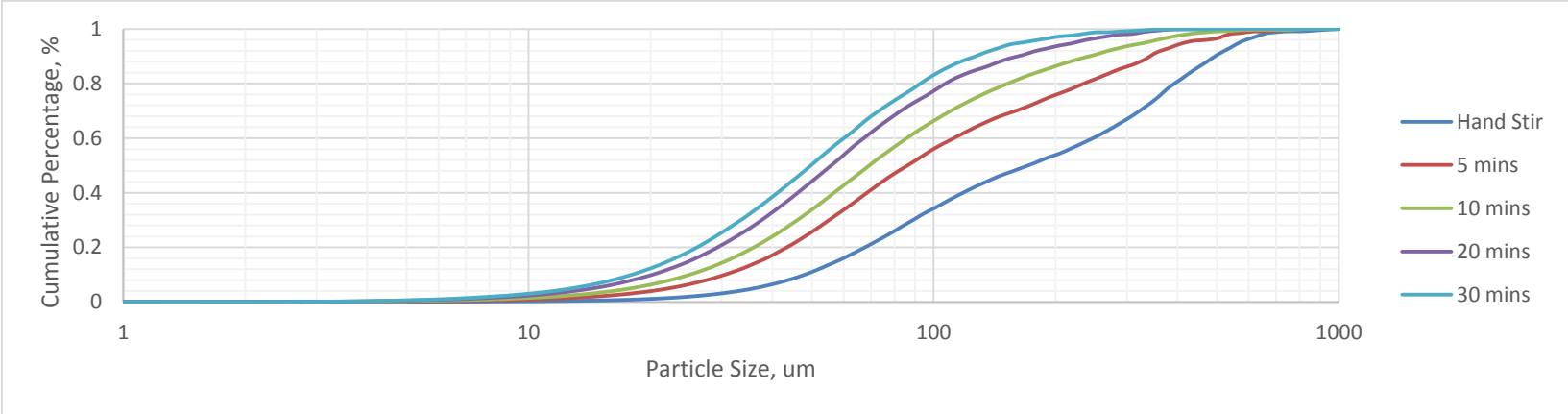

Figure A- 15 Cumulative PSD using MT with increasing shearing time for graphite regular

Appendix B: Preliminary Study on Relationship between Particle Size Distribution and Drilling Fluid Loss

B.1 INTRODUCTION

Numerous filtration models have been developed over last several decades, which help scientists and engineers to gain a better understanding of the filtration mechanism. Common parameters in these filtration models include, drilling fluid rheology, PSD, pore size distribution, local pressure/temperature and local flow rate. Drilling fluid rheology can be retrieved from mud reports while local pressure and flow rates can be determined from downhole sensors.

Filtration models and particle bridging theory reveal that PSD affects the filtration properties of drilling fluids. A preliminary experimental approach is adopted to determine the relationship between PSD and drilling fluid loss. If a quantitative relationship between PSD and drilling fluid loss could be determined, it will eliminate the need to perform the fluid loss test twice every day on the rigsite, which will highly improve the efficiency and accuracy of drilling fluid measurements.

B.2 LITERATURE REVIEW ON FILTRATION MODELS

As discussed in the Chapter 1, the uncontrolled filtration of drilling fluids can cause various problems. Filtration models describe the filtration process quantitatively and qualitatively, which will shed light on the proper control of the filtration Several experimental and theoretical works have been conducted in this area and a few of them are described in this section.

Ferguson classified drilling fluid filtrations into three types, namely static filtration, dynamic filtration and filtration beneath the bit. Static filtration occurs when the drilling fluid in not in circulation, i.e., during connecting pipes or changing drill bits. Thicker filter cake is formed during static filtration. When the drilling fluid starts to circulate, dynamic filtration takes place. The filter cake deposited from static filtration is eroded by the hydrodynamic forces and reaches an equilibrium thickness after a certain period of time. The rate of filtration increases at the beginning of dynamic filtration, and later on reaches a steady state. Even though the fundamental principles governing both filtration behaviors are the same, there is no direct relationship between static and dynamic filtration. Filtration beneath the bit is treated as a special case because filter cake does not form beneath the bit. Thus it is not controlled by the filter cake properties, but by how fast and well the particles can plug the formation ahead of the bit (Ferguson and Klotz 1954). Filtration beneath the bit will not be discussed in detailed in this Appendix.

Williams and Cannon built a filtration apparatus to observe the filtration behavior of different mud (Williams and Cannon 1938). Outmans performed experiments and found that the volume of filtrate is rather insensitive to the change in pressure and tried to explain

this phenomenon analytically by assuming a compressible filter cake (Outmans 1963). Jiao and Sharma modeled the mud cake growth, which was coupled with Darcy's Law, to describe steady state filtration (Jiao and Sharma 1994). Dewan and Chenevert approached the filtration problem numerically by including almost all the complexities of the filtration process into a simulator (Dewan and Chenevert 2001).

Williams and Cannon proposed an analytic solution for the steady state filtration in a linear flow based on Darcy's Law (Williams and Cannon 1938) and is given by

$$\frac{V}{A} = \sqrt{m\theta + c^2} - c$$

where V is the cumulative volume of filtrate, A is the area of filter, θ represents the time, m and c are constants which include the effect of the pressure drop across the cake, the viscosity of the filtrate and the resistance of the filter cake. This equation conforms to the classical filtration equation in chemical engineering. By utilizing Williams' wall-building tester, he was able to determine the constants by a graphical method for a Gulf coast drilling fluid at 100 psi pressure and at room temperature. They conducted series of experiments and found out that the degree of dispersion of solids and the distribution of particle sizes would affect the fluid loss volume due to the induced change in the filter cake properties. Even though the experiment conducted in the wall-building tester includes the circulation of drilling fluid, the effect of hydrodynamic forces is not discussed in this paper (Williams and Cannon 1938).

Later in 1952, Prokop investigated the effect of mud hydraulics on the formation of filter cakes. He identified four important aspects that govern the process, including the

solid deposition rate from the mud, the hydrodynamic force that erodes the mud cake, the resistance of filter cake to erosion and finally the change in filter cake properties due to erosion. The permeability of filter cake rarely changes during static filtration. While in the case of dynamic filtration, continuous circulation decreases the permeability of filter cake (Prokop 1952).

The experiment conducted by Ferguson in 1954 shows a positive relationship between the mud circulation velocity and the filtrate volume loss. Faster mud circulation velocity leads to a thinner filter cake. If the cake is too thin, it would not prevent the filtrate from invading the formation, resulting in an increase in the fluid loss (Ferguson and Klotz 1954). Bezemer and Havenaar's experiment showed similar results on the relationship between the equilibrium filtration rate, the equilibrium cake thickness and the shear rate at the cake surface (Bezemer and Havenaar 1966). For static filtration, Ferguson did not agree with Prokop. He assumed the filter cake to be a stack of thin layers and proposed that the static filtration is independent of pressure, because the permeability of the filter cake changes with pressure. However, his experimental results do not prove his hypothesis.

In 1963, Outmans qualitatively and quantitatively described dynamic and static filtration. He developed the filtration theory by comparing the formation of filter cakes to the consolidation theory in soil mechanics. He believed that the compressibility of filter cakes plays an important role in filtration behavior. The equation below describes static filtration as,

$$Q = \frac{2\alpha_1 P^{-\upsilon+1}}{(-\upsilon+1)erf(\lambda)}\sqrt{\frac{ct}{\pi\mu}}$$

where Q is cumulative filtrate volume, P is filtration pressure, α_1 is local filter cake compressibility at 1 psi solid pressure, c is coefficient of consolidation, t is time, μ is filtrate viscosity, υ and λ are constants defined for the convenience of calculation. For incompressible filter cake, α_1 is significantly smaller than 1. This equation is an approximation of the classical filtration equation. Outmans research study also provides a solution to the stress and the porosity distribution in the static filter cake (Outmans 1963).

Outmans believed that dynamic filtration consists of three stages (Figure B-1). During the first stage, filter cake builds up on the surface of wellbore. While at the second stage, the solids stop to accumulate on the surface of filter cake and the filtration rate starts to decrease. The filtration rate (q) approaches a constant at the third stage and is given by:

$$q = \frac{c}{\mu}\frac{\alpha_1 P^{-\upsilon+1}}{(-\upsilon+1)H}$$

where H is filter cake thickness. When the shear stress exerted on the filter cake surface, which removes the particles from the surface of the cake, equals the internal friction between the layers of the filter cake, which holds the particle in the place, it marks the end of the filter cake formation process.

Even though static and dynamic filtrations do not occur at the same time, the filter cake may contain deposits from both static and dynamic period, for example, a static filter cake accumulated on a dynamic filter cake. This type of filter cake is known as a composite filter cake. Filtration through the composite filter cake consists of two stages, first stage is erosion followed by a steady state.

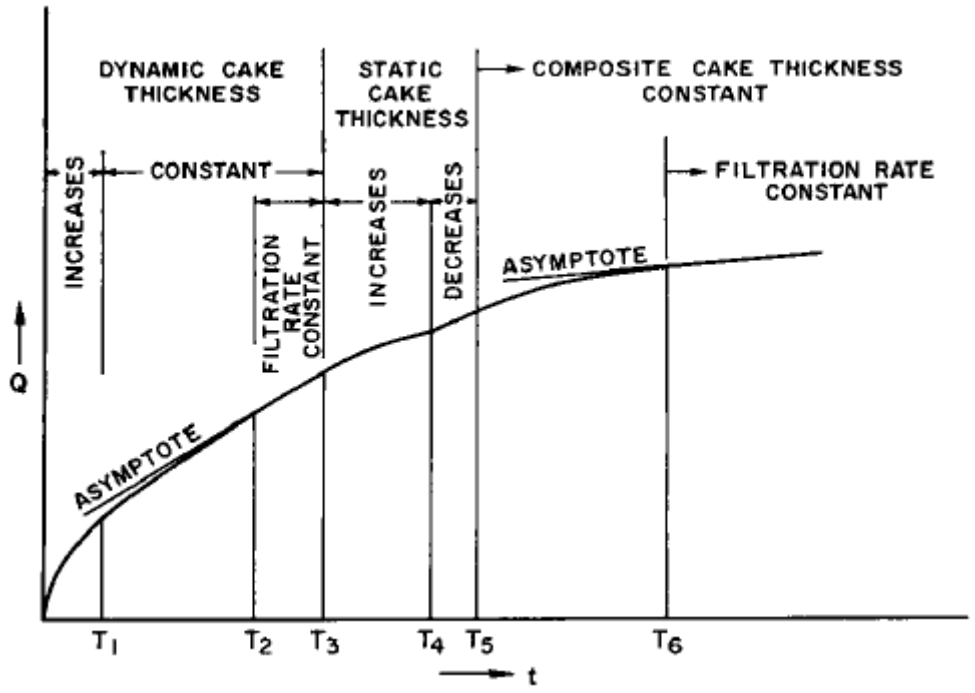

Figure B- 1 Dynamic filtration rate versus time for a complete cycle (Outmans 1963)

During dynamic filtration, both erosion and built up of filter cake occurs simultaneously. Jiao and Sharma offer an alternative perspective on mud cake formation in this period. They believed that there are two particle releasing mechanisms affecting the erosion and formation of filter cake. The particles deposited on the filter cake could be released either by sliding or by rolling. The force/torque balance and Darcy's law defines the steady state filtration process.

The first mechanism, sliding is dominated by friction and shear stress,

$$F_x \leq f F_y$$

where F_x is tangential force, F_y is drag force and f is the friction coefficient. Particles that satisfy the inequality deposit on the surface of filter cake. The mean particle size becomes smaller and smaller as filter cake grows, indicating the heterogeneity of the filter cake. When the filtration reaches a steady state, the filtration rate (q) could be described in terms of the maximum particle size in the filter cake,

$$q = \frac{2}{3}\left(\frac{\rho_f}{\rho_s}\right)^{1/n} \frac{(1-\phi)A}{k^{1/n}} \frac{R_{max}}{f^{1/n}} \tau_w^{1/n}$$

where ρ_f is the density of liquid, ρ_s is the density of solid, τ_w is a constant, A is the filter area, R_{max} is the maximum particle size that could be deposited on the surface, φ is the volume fraction of solids in the suspension, n is the flow index and k is consistency index of the suspension.

The second mechanism rolling is governed by torque balance,

$$T_y \leq T_x$$

where T_y is restraining torque and T_x is hydrodynamic torque.

The steady state filtration rate is described below and is proportional to the shear stress at the cake surface

$$q = \frac{2}{3}\left(\sqrt{3}\frac{\rho_f}{\rho_s}\right)^{1/n} \frac{(1-\phi)A}{k^{1/n}} R_{max} \tau_w^{1/n}$$

Dewan and Chenevert incorporated the equations describing the flow of filtrate and filter cake formation into a numerical simulator to predict the filtrate loss. Three methods are available for calculating the critical particle size that will adhere to a filter cake: Jiao and Sharma's, Fisher et al. and Lu and Ju's. Based on the validation of field mud, Fisher et al.'s method best approximates the dynamic filtrate rate. The simulator requires a variety

of mud parameters as the input, which could be determined from either filtration tests or analytical solutions (Dewan and Chenevert 2001).

Kozeny-Carman's equation described the flow through a pack of solids, unfortunately, it is only valid for laminar flow. However, by comparing this equation to Darcy's law, there emerges another way to calculate the permeability of a pack of solids. This method could be utilized to calculate the permeability of filter cake.

Jiao and Sharma provided a qualitative description for mud cake growth. Outmans' model is the most prevailing filtration model. Dewan and Chenevert's simulator is well accepted by the well logging world for predicting the degree of invasion of the filtrate into the formation (Wu et al. 2005). The fundamental difference in all the above-mentioned theories resides in the understanding of filter cake formation.

B.3 Particle Size Distribution vs Fluid Loss Experiment Procedure

In order to control the pore size distribution, we introduced an aloxite disk into the experiment (Table B-1). The aloxite disk is composed of aluminum oxide and silica. It is formed by packing particles of similar size to create a porous structure to simulate the subsurface formation. The experimental procedure is as follows:

1. Prepare 15 lab barrels (5.25 liters) of base mud as described in Table B-2.
2. Measure PSD of base mud with Malvern Mastersizer 2000.
3. Spilt 15 lab barrels of base mud into five equal portions, which is 3 lab barrels each.
4. Into each of the portions add 30 g of different glass microspheres while mixing the sample with a mixer. The particle size distribution of these glass microspheres are shown in Table B-3.
5. Transfer all the samples into separate mason jars and place all the mason jars in the roller oven for rolling at 150 °F for 16 hours. The sample undergoes an aging process to simulate downhole conditions.
6. Take all the mason jars out of the oven and transfer all the samples to designated stainless steel malt cups. Let all the samples cool down to room temperature.
7. Remix the mud samples for 10 minutes, which helps to agitate the mud.
8. Measure the density of mud.
9. Measure the rheological profile of mud at 120 °F.
10. Measure the fluid loss at 500 psi and 200 °F with different aloxite disks.
11. Measure the PSD with Malvern Mastersizer 2000.

Table B- 1 Properties of aloxite disk used in the experiment (OFITE Official Website)

No.	Mean Pore Throat (μm)	Permeability (Darcy)
1	12	0.85
2	20	3
3	50	15
4	120	40

Table B- 2 Base mud formulation

Material	Concentration, ppb	Mixing time at 8000 RPM, minutes
Xanthan Gum	1.2	8
Bio-Lose	2	10
Rev Dust	30	10
Barium Sulfate	70	10

Table B- 3 Particle size distribution of the various glass microspheres used in this study

	D10, μm	D50, μm	D90, μm
MS4	N/A	4	8
MS11	7	11	19
MS34	20	34	55
MS69	48	69	83

B.4 Particle Size Distribution vs Fluid Loss Experimental Results

The experimental procedure is detailed step by step in section B.3. The goal of this experiment is to quantitatively figure out the relationship between PSD and fluid loss.

According to section B.2, the quantity of fluid loss is dependent on the density of drilling fluids, rheological properties, PSD, the pore size distribution of formation and local pressure and temperature. The experiment was conducted at a differential pressure of 500 psi and at 200 °F temperature. Glass microspheres were chosen due to their shear resistance and inert behavior. They are used to modify the drilling fluid's PSD.

The glass microspheres used in the experiment are named after their D50. For example, MS69 refers to the glass microsphere with D50 of 69 μm. Base mud contained no glass microspheres. PSDs of drilling fluid samples shown in Figure B-2 are as expected. For instance, MS34 contained higher volume percentage of ~30 μm particles compared to that of base mud, which is clearly caused by the addition of glass microsphere with D50 of 34 μm.

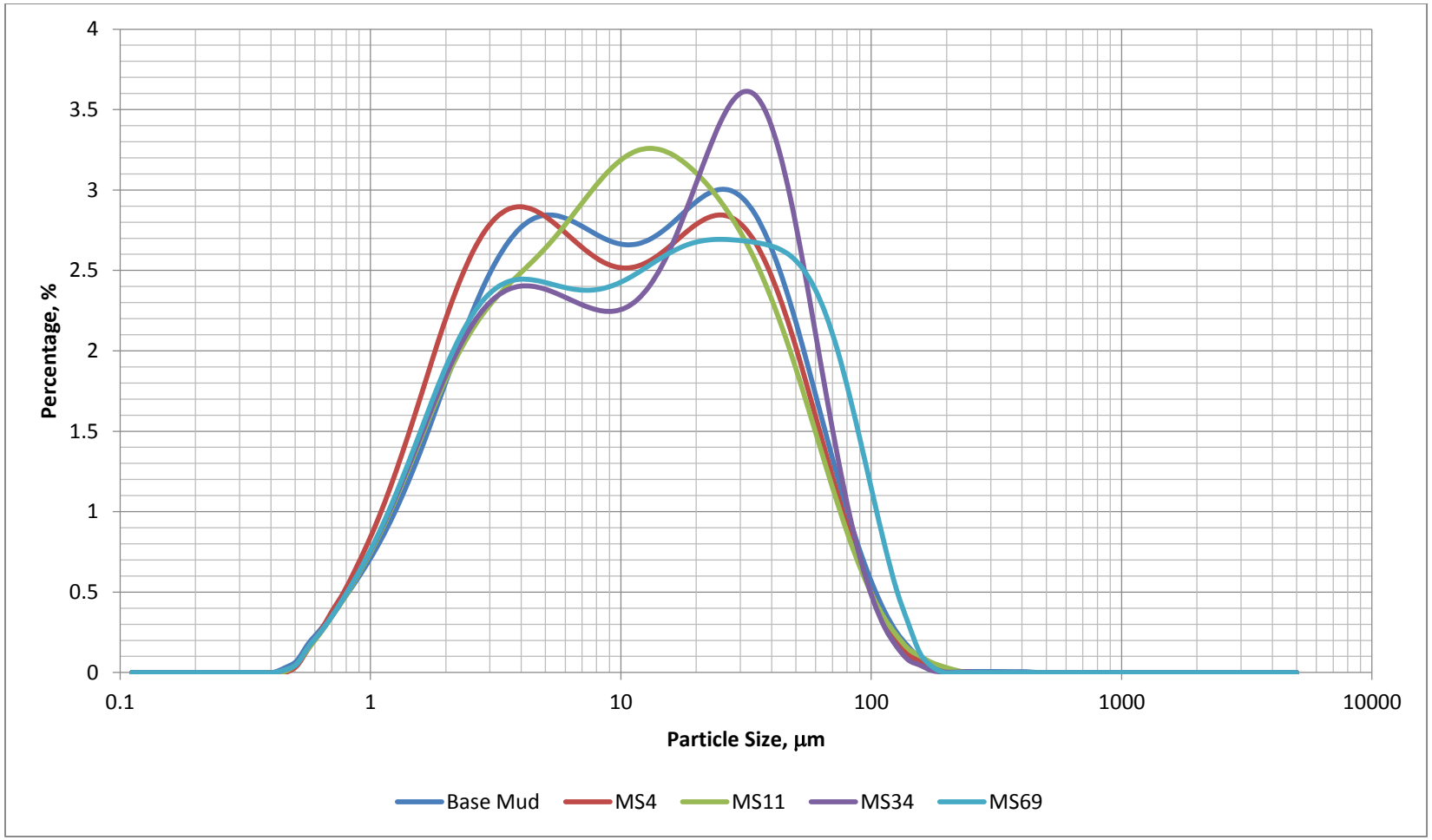

Figure B- 2 PSD of drilling fluid samples provided by Malvern Mastersizer 2000

The density of all drilling fluid samples were controlled around 10 ppg (see Table B-4). A slight increase in plastic viscosity (PV), a decrease in yield point (YP) and a decrease in 10 second gel strength are observed as glass microspheres were added into the base mud. Overall the rheological properties and density does not change as the glass microspheres were introduced into the system. Thus the change in fluid loss is more likely only due to the difference in PSD of drilling fluid samples and pore size distribution of aloxite disks.

Table B- 4 Density and rheological properties of drilling fluid with different glass microspheres

	MS69	MS34	MS11	MS4	No MS
Density, ppg	10.03	9.96	10	9.85	9.85
PV	11.2	10.3	12.1	11.6	9.5
YP	21.8	24.5	22.5	22.9	25.8
10 sec gel	5.4	5.9	5.4	5.6	6.7
10 min gel	8.3	8.9	9.8	9.2	8.7
Dial Readings @ 120 °F					
600 RPM	44.2	45.1	46.7	46.1	44.8
300 RPM	33	34.8	34.6	34.5	35.3
200 RPM	27.9	30	30	29.6	31.2
100 RPM	21	23	22.9	22.6	24
6 RPM	7.6	8.1	8.6	7.6	9.3
3 RPM	5.9	6.7	7	6.4	7.3

Based on the results shown in Table B-5, PSD of the base mud has sufficient fluid loss control. Table B-5 shows that in most cases, the introduction of glass microspheres leads to a further increase in the value of fluid loss. However, the differences in the increases might be due to the varying values of PSD. MS69 sample yields the lowest fluid loss for 12, 20 and 50 μm aloxite disk throat sizes. Taking a closer look at the difference in PSD, it was found that MS69 sample has a broader PSD and has a higher concentration of larger particles. Meanwhile, the higher fluid loss observed for MS11 and MS4 for 12, 20 and 50 μm throat sizes might be due to an increase in the volume of finer particles in the system.

One test result is not sufficient to quantitatively correlate the PSD of drilling fluid with fluid loss. However, the results shown in this appendix indicate that the effect of PSD on fluid loss might be more significant than what was traditionally expected. Even without a significant change in PSD, the fluid loss could still change from 5.2 cc to 7.2 cc in a water based mud. More tests have to be conducted to develop a quantitative relationship between PSD and fluid loss, by taking several factors in to consideration such as rheological properties, formation characteristics and downhole conditions.

Table B- 5 High pressure high temperature fluid loss results of drilling fluid samples with different glass microspheres

Mean Pore Throat of Aloxite Disk, μm	Fluid Loss (ml)				
	MS69	MS34	MS11	MS4	Base Mud
12	5.2	5.4	7.2	7.4	5.8
20	4.3	4.7	7.3	6.8	3.7
50	5.8	7	6.8	9.8	4
120	7.6	N/A	1.8	2.3	2.2

B.5 OBSERVATIONS

PSD of drilling fluid is an important factor because of its impact on fluid loss control, lost circulation mitigation and even wellbore strengthening. The goal of the experiment presented in this appendix was to obtain a correlation between PSD and fluid loss. In this study, it was shown that the PSD has a direct impact on fluid loss. More experimental tests have to be conducted in order to develop a quantitative correlation between PSD, pore size distribution and fluid loss, especially to understand the particle plugging mechanism that leads to sealing of formation pores. The correlation could help with lost circulation mitigation as well. Prevention is better than expensive corrections. If the core information could be retrieved or if a possible lost circulation scenario is predicted, the correlation or say the understanding of how the particle plugs and seals the pores could determine the proper selection of bridging material, saving time, saving cost or even saving lives.

Bibliography

Abrams, A. 1977. “Mud Design To Minimize Rock Impairment Due To Particle Invasion.” *Journal of Petroleum Technology* 29 (5): 586–92. doi:10.2118/5713-PA.

Allen, Terence. 1996. *Particle Size Measurement: Volume 1: Powder Sampling and Particle Size Measurement*. Particle Technology Series. Springer Netherlands. https://books.google.com/books?id=5rBP5OFdrvkC.

———. 2003. *Powder Sampling and Particle Size Determination*. Elsevier.

American Petroleum Institute. Production Department. 1990. *Recommended Practice Standard Procedure for Field Testing Water-Based Drilling Fluids*. Vol. 13. American Petroleum Institute.

ASME, Fred Growcock, and Tim Harvey. 2005. *Drilling Fluids Processing Handbook*. *Drilling Fluids Processing Handbook*. Elsevier. doi:10.1016/B978-075067775-2/50003-2.

Beare, Steve, and Tracey Jane Ballard. 2013. “Particle Size Analysis For Sand Control Applications.” In *SPE European Formation Damage Conference*. Noordwijk, The Netherlands: Society of Petroleum Engineers. doi:10.2118/165119-MS.

Bezemer, C., and I. Havenaar. 1966. “Filtration Behavior of Circulating Drilling Fluids.” *Society of Petroleum Engineers Journal* 6 (4). doi:10.2118/1263-PA.

Burdine, Nt, Ls Gournay, and Pp Reichertz. 1950. “Pore Size Distribution of Petroleum Reservoir Rocks.” *Journal of Petroleum …* 2 (07): 195–204. http://www.onepetro.org/mslib/servlet/onepetropreview?id=SPE-950195-G.

Canty. 2012. “Particle Counter.” http://commons.wikimedia.org/wiki/File:Vision_Based_Particle_Counter.jpg.

Cargnel, R. D., and J. P. Luzardo. 1999. “Particle Size Distribution Selection of CaCO3 in Drill-In Fluids : Theory and Applications.” In *Latin American and Caribbean Petroleum Engineering Conference*. Caracas, Venezuela.

Cospheric LLC. 2014. “Material Data Sheet.”

Cowlard, F. C., and J. C. Lewis. 1967. “Vitreous Carbon - A New Form of Carbon.” *Journal of Materials Science* 2 (6): 507–12. doi:10.1007/BF00752216.

Darley, Henry C H, and George Robert Gray. 1988. *Composition and Properties of Drilling and Completion Fluids*. Gulf Professional Publishing.

Davidson, Michael W, and Mortimer Abramowitz. 1999. "Optical Microscopy." *Encyclopedia of Imaging Science and Technology*. Wiley Online Library.

Dewan, J T, and M E Chenevert. 2001. "A Model for Filtration of Water-Base Mud During Drilling : Determination of Mudcake Parameters" 42 (3): 237–50.

Dick, M.a., T.J. Heinz, C.F. Svoboda, and M. Aston. 2000. "Optimizing the Selection of Bridging Particles for Reservoir Drilling Fluids." *SPE International Symposium on Formation Damage*, 1–8. doi:10.2118/58793-MS.

Ferguson, C.K., and J.a. Klotz. 1954. "Filtration From Mud During Drilling." *Journal of Petroleum Technology* 6 (2): 30–43. doi:10.2118/289-G.

Gatlin, Carl, and Charles Nemir. 1961. "Some Effects of Size Distribution on Particle Bridging in Lost Circulation and Filtration Tests." *Journal of Petroleum Technology* 13 (6): 575–78. doi:10.2118/1652-G.

Gordon, Roy G. 2000. "Criteria for Choosing Transparent Conductors." *MRS Bulletin* 25 (08): 52–57. doi:10.1557/mrs2000.151.

Goud, Milap Chand, and Givi Joseph. 2006. "Drilling Fluid Additives and Engineering to Improve Formation Integrity." In *IADC/SPE Driling Conference and Exhibition*. Mumbai, India.

Groen, Johan C, Louk A.A Peffer, and Javier Pérez-Ramírez. 2003. "Pore Size Determination in Modified Micro- and Mesoporous Materials. Pitfalls and Limitations in Gas Adsorption Data Analysis." *Microporous and Mesoporous Materials* 60 (1-3): 1–17. doi:10.1016/S1387-1811(03)00339-1.

He, Wenwu, and Mike Stephens. 2011. "Bridging Particle Size Distribution in Drilling Fluid and Formation Damage." *SPE European Formation Damage Conference*, no. June: 7–10. doi:10.2118/143497-MS.

HORIBA Instruments Inc. 2014. "A Guidebook To Particle Size Analysis."

Jiao, D., and Mukul M. Sharma. 1994. "Mechanism of Cake Buildup in Crossflow Filtration of Colloidal Suspensions." *Journal of Colloid and Interface Science*. doi:10.1006/jcis.1994.1060.

Karimi, Moji. 2013. “Drill-Cuttings Analysis for Real-Time Problem Diagnosis and Drilling Performance Optimization.” In *SPE Asia Pacific Oil and Gas Conference and Exhibition*. Jakarta, Indonesia: Society of Petroleum Engineers. doi:10.2118/165919-MS.

Kippax, Paul. 2005. “Measuring Particle Size Using Modern Laser Diffraction Techniques.” *Chemie. De*, 1–2.

Kumar, Arunesh, Kuhan Chellappah, Mark Aston, Roman Bulgachev, and B P Plc. 2013. “Quality Control of Particle Size Distributions.” In *SPE European Formation Damage Conference & Exhibition*. Noordwijk, The Netherlands: Society of Petroleum Engineers.

Lide, David R. 2005. “Hardness of Minerals and Ceramics.” In *CRC Handbook of Chemistry and Physics*, Internet V, 2313–14. Boca Raton, FL: CRC Press. http://www.hbcpnetbase.com.

Mahajan, Naresh C., and Bruce M. Barron. 1980. “Bridging Particle Size Distribution: A Key Factor in the Designing of Non-Damaging Completion Fluids.” In *SPE Formation Damage Symposium*. Bakersfield, California.

Malvern Instruments Ltd. 2015. “Mastersizer 2000.” Accessed June 5. http://www.malvern.com/en/support/product-support/mastersizer-range/mastersizer-2000/.

———. 2007. *Mastersizer 2000 User Manual*.

———. 2012. “A Basic Guide to Particle Characterization.” *Inform White Paper*, 1–26.

McCave, I. N., R. J. Bryant, H. F. Cook, and C. A. Coughanowr. 1986. “Evaluation of a Laser-Diffraction-Size Analyzer for Use with Natural Sediments: RESEARCH METHOD PAPER.” *Journal of Sedimentary Research* 56 (4): 561–64. doi:10.1306/212F89CC-2B24-11D7-8648000102C1865D.

Mettler-Toledo International Inc. 2015. “FBRM Technology.” Accessed June 5. http://us.mt.com/us/en/home/supportive_content/specials/Lasentec-FBRM-Method-of-Measurement.html.

Mohamed, Monir. 2011. “Engineered Particle Size Distribution While Drilling Helped Minimize Wellbore Damage in Sandstone Reservoirs.” *Middle East*.

Outmans, H.D. 1963. “Mechanics of Static and Dynamic Filtration In the Borehole.” *Society of Petroleum Engineers Journal* 3 (3). doi:10.2118/491-PA.

Prokop, C.L. 1952. “Radial Filtration of Drilling Mud.” *Journal of Petroleum Technology* 4 (1): 5–10. doi:10.2118/143-G.

Ronaes, Egil, Truls Hosy Fossdal, and Tore Stock. 2012. “Real-Time Drilling Fluid Monitoring and Analysis - Adding to Integrated Drilling Operations.” In *IADC/SPE Driling Conference and Exhibition*. San Diago, Califronia: Society of Petroleum Engineers. doi:10.2118/151459-MS.

Scott, Paul Daniel, David Hale Beardmore, Zack Lee Wade, Eddie Evans, and Krista Deanne Franks. 2012. “Size Degradation of Granular Lost Circulation Materials.” In *IADC/SPE Driling Conference and Exhibition*. Society of Petroleum Engineers. doi:10.2118/151227-MS.

Smith, P. S., S. V. Browne, T. J. Heinz, and W. V. Wise. 1996. “Drilling Fluid Design to Prevent Formation Damage in High Permeability Quartz Arenite Sandstones.” In *SPE Annual Technical Conference and Exhibition*. Denver, CO.

Sympatec System Particle Technology. 2015. “Ultrasonic Extinction for Particle Size Analysis in Concentrated Suspensions from 10 Nm to 3 Mm.” Accessed July 5. https://www.sympatec.com/EN/UltrasonicExtinction/UltrasonicExtinction.html.

Valsecchi, Pietro. 2014. “On the Shear Degradation of Lost-Circulation Materials.” *SPE Drilling & Completion* 29 (03). Society of Petroleum Engineers: 323–28. doi:10.2118/163512-PA.

Vickers, Stephen, Martin Cowie, Tom Jones, and Allan J Twynam. 2006. “A New Methodology That Surpasses Current Bridging Theories to Efficiently Seal a Varied Pore Throat Distribution as Found in Natural Reservoir Formations.” *Wiertnictwo Nafta Gaz* 23/1: 501–15.

White, Robert J. 1956. “Lost-Circulation Materials and Their Evaluation.” In *Drilling and Production Practice*. New York: American Petroleum Institute.

Williams, Milton, and G. E. Cannon. 1938. “Evaluation of Filtration Properties of Drilling Mud.” In *Drilling and Production Practice*. Amarillo, Texas: American Petroleum Institute.

Wu, J, C Torres-Verdín, K Sepehrnoori, and M Proett. 2005. “The Influence of Water-Base Mud Properties and Petrophysical Parameters on Mudcake Growth, Filtrate Invasion and Formation Pressure.” *Petrophysics* 46 (1): 14–32.

Xu, Renliang. 2002. *Particle Characterization : Light Scattering Methods*. Particle Technology Series. New York: Kluwer Academic.

http://ezproxy.lib.utexas.edu/login?url=http://search.ebscohost.com/login.aspx?direct=true&db=nlebk&AN=67605&site=ehost-live.